UiT Norges arktiske universitet

Faculty of Science and Technology

Department of Geosciences

Molecules and Morphotypes – Exploring benthic foraminiferal biodiversity in seep-influenced habitats

Villads Dyrved Holm

Master's Thesis in Geology [GEO-3900]

May 2023

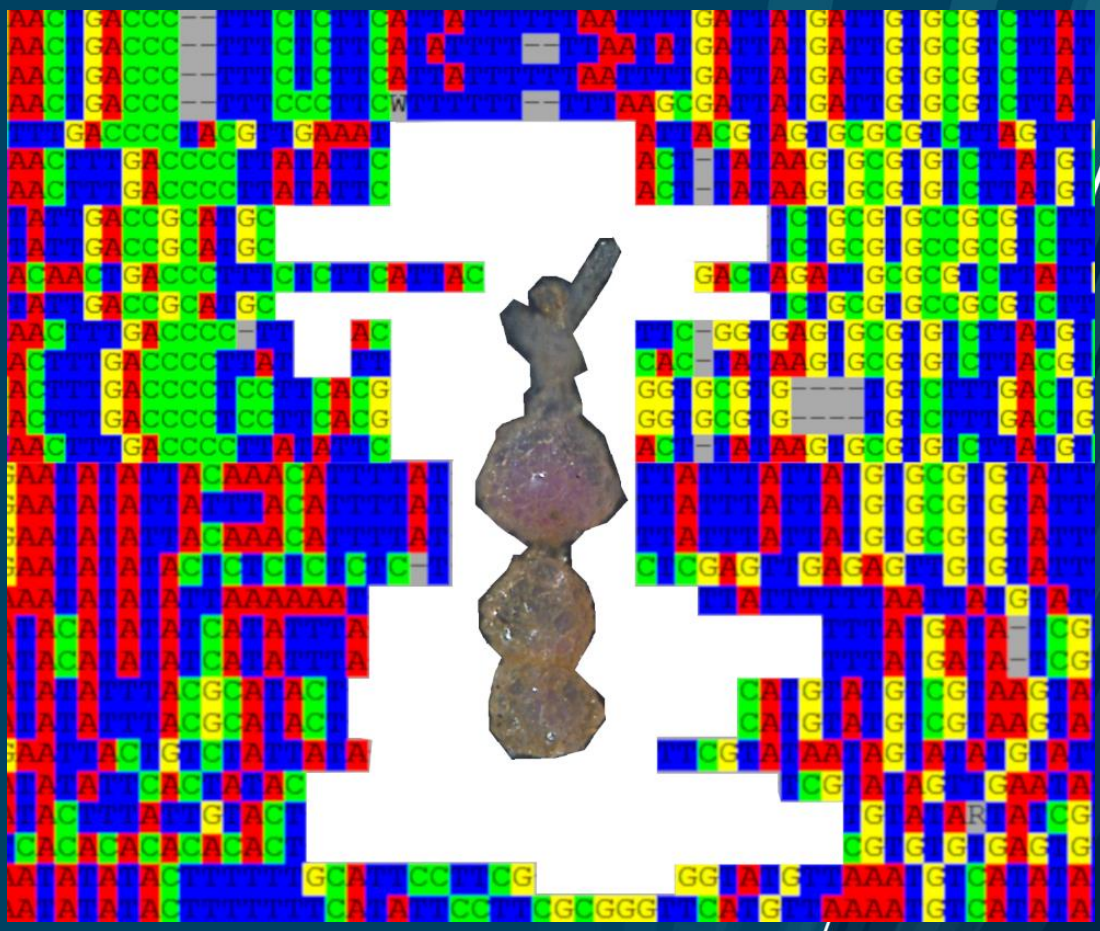

Abstract

Beneath the seafloor, methane, a potent greenhouse gas, is trapped in ice-like structures, prone to destabilization and gas release in a warming climate. Gas releases through the seabed concentrated in seeps, creating unique ecosystems, hostile to some lifeforms but able to sustain others.

Foraminifera have proved useful in biodiversity and ecosystem quality assessment due to their ubiquity in marine environments, fast turnover rate and high degree of specialization. Morphology-based studies however tend to ignore soft-shelled monothalamous foraminifera, despite their substantial contributon to benthic communities, potentially resulting in a loss of biodiversity. Molecular-based studies can be plagued by lacking databases, leading to a large amount of undetermined sequences, as is the case with seep-related foraminifera.

In this thesis, morphology- and molecular-based approaches are used to investigate foraminifera sampled from different seep-related microhabitats at Vestnesa Ridge. For the first time, soft-shelled and agglutinated benthic communities in this area are characterized. A drop in diversity is observed with proximity to the hostile geochemical conditions of microbial mats, primarily through a loss of organic-walled and multilocular agglutinated taxa. Select saccamminid and psammosphaerid taxa seem to thrive in this environment. Most strikingly, two previously undescribed saccamminid taxa dominate the assemblage at the microbial mat, comprising a combined 40% of the total community. These taxa are absent in the other microhabitats, indicating a high degree of specialization to the seep environment, like the hypothesized symbiosis between *Melonis barleeanus* and methanotrophic bacteria.

These two taxa as well as *Psammosphaga sp.* are highlighted here as potential candidates for future barcoding studies of seep-related foraminifera.

SSU ribosomal DNA sequences were obtained from hard-shelled foraminfera living at the reference site, the in-site reference and the tubeworm zone, representing the first of their kind from these environments. Although the barcoded specimens show little to no genetic variation, the sequences belonging to *Stainforthia cf. fusiformis* differ from other *Stainforthia*-like sequences obtained through eDNA metabarcoding of the site, indicating the presence of two genetically distinct *Stainforthia spp.*, something that would likely have been overlooked in studies based on morphological data alone.

Foreword

Many people have helped me throughout this process, and though not all are named here, no one is forgotten.

I would like to acknowledge the AKMA project for financially supporting the laboratory work conducted in Geneva.
I would like to thank Maria Holzmann of the University of Geneva and my co-supervisor, Jan Pawlowski of ID-gene ecodiagnostics for invaluable guidance in the laboratory, on the R/V Kronprins Håkon and in e-mail correspondance.

I would like to thank Inés Andrea Barrenechea Angeles for great and constructive feedback and for help with the phylogenetic analyses.

Trine Dahl, Ingvild Hald and Karina Monsen all deserve mention for their patience with me and extending my time with the compound microscope over and over again.

Julie Marie Seime Sortland, Anita Holmgren and Sari Elena Dötterer deserve mention here for their unwavering moral support through the good times and the bad.

Last but not least, heartfelt gratitude goes out to my supervisor, Giuliana Panieri, for allowing me great opportunities to expand my academic knowledge and know-how, for introducing me to great and interesting people, and for believing in me over the course of this project.

Contents

1 Introduction

1.1 A warming Arctic

In the Arctic, surface air temperatures are increasing at an alarming rate (1,9 times greater than the global mean, as per the Intergovernmental Panel on Climate Change (IPCC)(Winton, 2006)), a phenomenon known as Arctic amplification (Fig. 1) (Serreze & Barry, 2011). There are a variety of drivers for this phenomenon, including but not limited to the albedo feedback, changes to the sea ice extent and changes in cloud cover (Serreze & Barry, 2011).

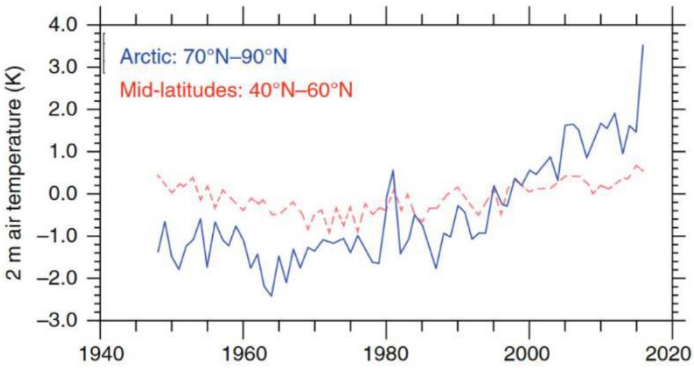

Figure 1: Near-surface air temperature departures from normal (relative to 1981-2010). Source: Francis et al. 2017.

The impact of the Arctic amplification is thought to reach beyond the already climatically sensitive ecosystems in the high latitudes, and changes in atmospheric circulation caused by the amplification have been hypothesized to be linked to increased frequency in extreme weather events in the mid-latitudes (Cohen *et al*. 2014). In order to better understand and deal with the changing climate, the understanding of the fate of greenhouse gases (GHGs) is crucial knowledge.

1.2 Methane

Methane (CH_4) is a potent GHG, up to 84 times more potent than carbon dioxide (CO_2) when considered over a 20-year period after release (Jackson *et al*. 2019). The seafloor of the Arctic Ocean and the Barents Sea are known to be littered with seeps, areas where gases including CH_4 discharge through the sediments (Mau *et al*. 2017; Yao *et al*. 2020). The aim of the AKMA project (Advancing Knowledge of Methane in the Arctic) , a collaboration between UiT – The Arctic University of Norway in Tromsø and the Woods Hole Oceanographic Institute in USA, is to gain insight into the effect of CH_4 discharge on Arctic and global climate, as well as local ecosystems.

Below the seafloor, CH_4 is sequestered in ice-like structures known as gas hydrates or clathrates (Buffett & Archer, 2004). Clathrates are climatically sensitive, with ocean warming leading to destabilization and gas release (Joung *et al*. 2022**)**. If the released CH_4 reaches the atmosphere as a GHG, this can potentially result in a positive feedback loop where increased gas release leads to increased warming of the ocean and so forth. Though Joung *et al.* (2022) found the exchange between fossil (clathrate-bound) CH_4 and the atmosphere to be negligible in mid-latitude oceans, the large amounts of trapped CH_4 might impose problems in the warming Arctic of the future.

1.3 Foraminifera

The phylum Foraminifera (d'Orbigny, 1826) is a large group of protists, highly successful and present in both marine, terrestrial and freshwater environments (Pawlowski & Holzmann, 2002**)**. In the marine realm, they are ubiquitous and abundant in benthic communities (Gooday *et al.* 2005). Within the field of paleoceanography, foraminifera have proved useful proxies for reconstruction of water column temperature, salinity, sea-ice extent etc., due to their sensitivity to environmental parameters (Kucera, 2007). In relation to paleo-methane seepage, the study of past CH_4 emission, the stable isotope composition of the calcareous test of foraminifera is a useful proxy **(**Panieri, 2006; Panieri *et al*. 2016). Some foraminifera utilize carbonate from their surroundings for biomineralization, including bicarbonate depleted in ^{13}C, produced through the anaerobic oxidation of CH_4 by microbial methanotrophs at the sulfate-methane transition zone (SMTZ) (Knittel & Boetius, 2009), leading to depleted $\delta^{13}C$ signatures in the fossil record.

Foraminifera are also utilized in modern-day bio-diversity and bio-monitoring studies. The FOBIMO initiative (FOraminiferal BIo-MOnitoring, Schönfeld *et al*. 2012) highlights their utility as indicators of environmental change, due to high turnover rates, a high degree of specialization and well-preserved fossil record.

Examples of their utility include a study on the impact of fish farming on benthic communities. (Pawlowski *et al.* 2014) utilized environmental DNA (eDNA) metabarcoding to characterize the foraminiferal assemblage along environmental gradients, and found high variations, and a decrease in species richness in communities proximal to fish farming sites. They conclude that metabarcoding of foraminifera has great potential in monitoring the

quality of marine ecosystems, as it is less costly and more time-efficient than traditional morphology-based studies.

Frontalini *et al*. (2020) also compared the two methodologies (metabarcoding and morphology-based assessment), in a study of the environmental impact of three offshore gas platforms. They found that the two methods gave congruent results in terms of biodiversity indices (Fig. 2). When it came to the taxonomical compositions of the two datasets, however, the dataset obtained from metabarcoding included a high amount of sequences belonging to soft-shelled molothalamous species. Amongst the monothalamous sequences were several molecular operational taxonomical units (MOTUs) with potential as bioindicator species for pollution. The authors also high-lighted the cost and time-efficiency of metabarcoding studies compared to classical morphology-based studies.

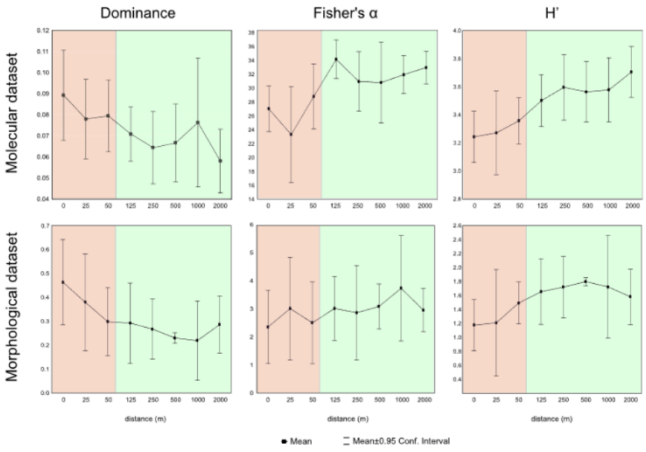

Figure 2: Simpson's Dominance, Fisher's α and Shannon-Weiner (H'), calculated from molecular and morphological data sets. Source: Frontalini et al. 2020.

Pawlowski *et al*. (2022, unpublished progress report commisioned by Giuliana Panieri) used eDNA metabarcoding to study foraminiferal diversity at oil and gas seeps in the Arctic Ocean. They found a large number of undetermined sequences, but also an abundance of *Stainforthia*-like sequences in the CH_4 site, indicating a potential bioindicator species. They also concluded, given the high amount of undetermined sequences, that further barcoding studies are necessary to explore the diversity at these sites.

1.4 Barcoding foraminifera

Barcoding is the process of identification of species using short gene sequences (Pawlowski & Holzmann, 2014). In foraminifera, the short subunit (SSU) 18S gene is often used, as it contains several hypervariable regions, enabling differentiation between species. In particular, the SSU ribosomal DNA comprises six variable regions, three of which are specific to

foraminifera (37f, 41f, 47f) and the other three also found in other eukaryotes (Pawlowski & LeCroq, 2010).

Identification through barcoding can overcome some challenges where morphology-based identification falls short. Phenotypic plasticity, the variation in morphological features, can make it difficult to distinguish between species, as members of the same species can display different ecophenotypes based on environmental conditons (Pawlowski & Holzmann, 2014). Morphological studies can also overlook cryptic speciation, morphological congruence between different species.

Metabarcoding studies rely on a solid database of sequences assigned to species. As mentioned before, the metabarcoding study of seep sites in the Arctic revealed many undetermined sequences. It is therefore of great importance to sequence more foraminifera from these environments, in order to support future biomonitoring studies.

1.5 The Arctic seep habitat

Argentino *et al*. (2022) employed seafloor imagery and sediment coring to study the environment at an arctic seep in the Barents Sea. They found a concentric zonation of microhabitats, centered around the area with the highest CH_4 flux (Fig. 3). The center is inhabitated only by microbial mats of methanotroph archaea and sulfate-reducing bacteria, tolerant to the hostile conditions present In this area (Argentino *et al*. (2022). The SMTZ is closest to the seafloor, and the sulfate concentration and pCO^2 is too high to sustain most life.

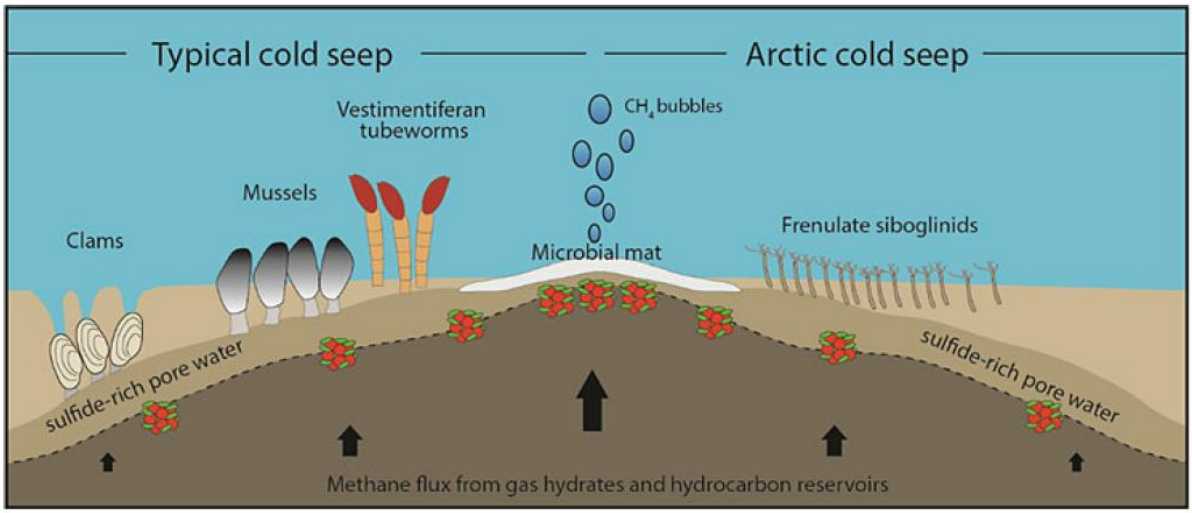

Figure 3: Sketch of typical zonation of communities at cold seeps. Source: Argentino et al. 2022.

Away from the center, the SMTZ deepens and sulfide production is lower. These outer zones are inhabited by frenulate sibuglinids (Tubeworms) and chemosynthetic bivalves.

1.6 Foraminiferal assemblages at Vestnesa Ridge

Dessandier *et al*. (2019) examined faunal assemblages of benthic foraminifera as well as environmental conditions in 12 pushcores collected inside and outside of microbial mats in the Lunde and Lomvi pockmarks of Vestnesa Ridge. Rose Bengal staining was used to distinguish between recently deceased and dead specimens. The study described three different

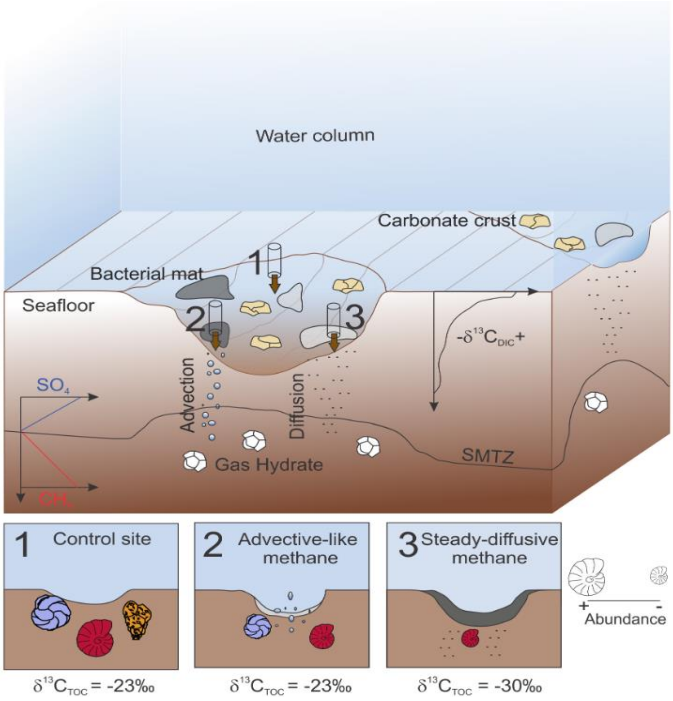

Figure 4: Cartoon summarizing the microhabitats and findings of Dessandier et al. 2019. Source: Dessandier et al. 2019.

environmental conditions, characterized by different flow regimes, and with different faunal characteristics. A cartoon summarizing their findings can be seen in Fig. 3. Microbial communities differed in the two flow regimes and were absent in the sediments not affected by seepage (Dessandier *et al*. 2019). In unstable environments characterized by pulses of advective-like methane, microbial communities were likely dominated by *Arcobacter sp.* and *Thiomargarita sp.*, forming black and grey microbial mats. In the environments characterized by a steady flow of diffusive methane, microbial communities were likely dominated by filamentous *Beggiatoa sp.*, forming white mats and known to thrive in more stable conditions (Dessandier *et al*. 2019). The benthic (0-1 cm) foraminifera communities also differed between the microhabitats. The control core (no seepage) displayed the highest faunal density and diversity (Dessandier *et al*. 2019). Notably, agglutinated species were prominent in this core, in line with previous studies done on Arctic foraminifera assemblages (Gooday *et al*. 2005). Agglutinated species were however absent from the seep-related cores (Fig. 3), explaining the lower diversity. Agglutinated species show a preference for oligotrophic

(deficient of nutrients) environments, and might not tolerate the eutrophic conditions sustained by the high amounts of organic carbon provided by e.g. the microbial communities in methane-charged sediments (Heinz et al. 2005; Dessandier *et al*. 2019).

Foraminifera assemblages also differed in the two different flow regimes. Abundance and diversity were generally found to be higher in the habitats characterized by advective pulses of methane (Fig. 3; Dessandier *et al*. 2019). Common Arctic calcareous species were observed across all microhabitats, specifically *Buccella frigida* (Cushman, 1922a), *Melonis barleaanus* (Williamson, 1858) *and Cassidulina sp.* These species are known to be tolerant of eutrophic environments, thriving with the ample availability of food sourced from microbes. Diversity was lowest in the microhabitat characterized by a steady flow of diffusive methane (Dessandier *et al*. 2019), which might be too toxic to sustain a benthic community. *Melonis barleaanus* dominated these faunas and might be tolerant of higher sulfide contents (Dessandier *et al*. 2019). *Melonis barleeanus* specimens collected from Vestnesa Ridge have been observed in association with methanotroph bacteria (Bernhard & Panieri, 2018), and while no conclusions have been made on any possible symbiosis between the organisms, it is possible that the specific microbial communities sustained in methane-charged sediments have an impact on the benthic foraminifera fauna. The study found no endemic species related to seep sites, in line with previous studies on the subject matter (See Dessandier *et al*. 2019 and references therein).

1.7 Objective of the study

This thesis aims to advance the knowledge on foraminifera inhabiting the extreme environments characterized by methane seepage. This is done in two ways: Through morphological identification of the understudied soft-shelled monothalamous forams inhabiting the methane seeps and related microhabitats of Vestnesa Ridge, and through barcoding of select hard-shelled foraminifera from the same environment. It is the hope that the findings in this thesis can aid in identifying prospective candidate species/morphospecies for future barcoding studies, enabling the better application of metabarcoding biomonitoring in seeps and other extreme environments.

2 Geological setting

2.1 Vestnesa Ridge

Vestnesa Ridge is a ~100 km long sediment drift situated in the eastern Fram Strait, between Greenland and Spitsbergen (Fig. 4), where it connects the west Svalbard continental margin to the east (Vogt *et al*. 1994**)**. The area has two major climate-regulating currents flowing through, the northbound North Atlantic Current and the southbound East Greenland Current (Dessandier *et al*. 2019), the former shaping the contouritic deposits through its local branch, the West Spitsbergen Current (Bünz *et al*. 2012). Since the discovery of several pockmarks in 1994, the gas hydrate province in this area has been studied in great detail **(**see, e.g., Vogt *et al*. 1994; Bünz *et al*. 2012; Plaza-Faverola *et al*. 2015**;** Panieri *et al*. 2017; Dessandier *et al*. 2019), uncovering seabed structures due to gas seepages, gas release, seep-related faunal dynamics and massive carbonate crusts. At approximately 79° N, Vestnesa Ridge is one of the world's northernmost gas hydrate provinces on continental margins (Bünz *et al*. 2012).

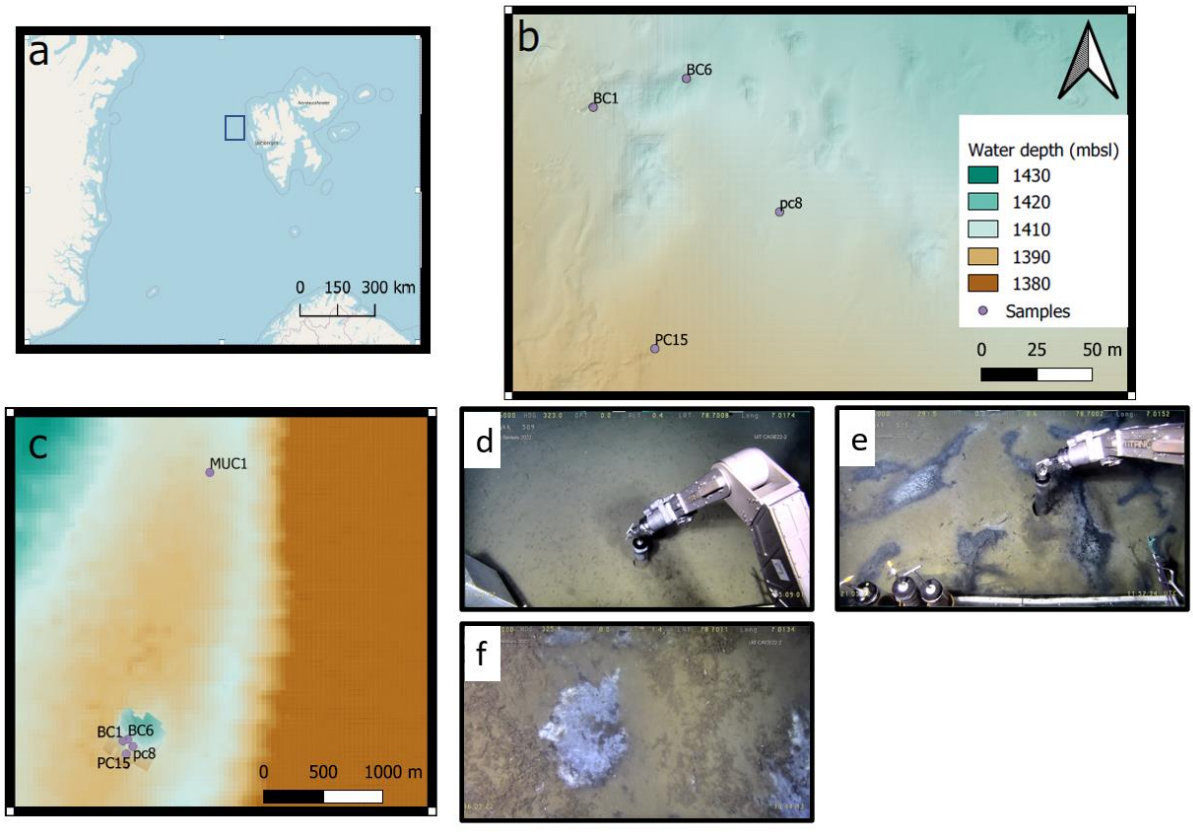

Figure 5: Map of the studied area. a: Overview map with the approximate location of Vestnesa Ridge marked by a square. b: Map of sampling locations. c: Map showing Reference site in relation to the other sample locations. d: Collection of PC8 at the in-site reference. e: Collection of PC15 at the microbial mats. Notice the grey-black color of the mats. f: Transition between microbial mat and tubeworm zone.

Vestnesa Ridge is located on young and relatively hot crust originating from the Molloy Ridge to the southwest, the northernmost extension of the Mid-Atlantic ridge system, where heat flow values are 2 to 3 times higher than in the nearby Barents and Mid Norwegian Seas (Vogt *et al*. 1994; Bünz *et al*. 2012). Furthermore, the Vestnesa Ridge gas hydrate province occurs at depths of 1200-1300 m, where the dissociation of hydrates due to changes in ocean temperature does not explain gas release (Plaza-Faverola *et al*. 2015), in contrast to the Barents and Mid Norwegian Seas.

Buried mounds observed across Vestnesa Ridge indicate a periodicity to gas expulsion (Plaza-Faverola *et al*. 2015). Vestnesa Ridge is situated in proximity to the Molloy and Knipovich Ridges as well as the Spitsbergen Transform Fault, and tectonic stresses from these regions appear to have influenced the seep evolution (Plaza-Faverola *et al*. 2015).

Periodicity of seep activity as evidenced by the buried mounds on the order of some hundred thousand years and seem to coincide with glacial intensification (Plaza-Faverola *et al*. 2015).

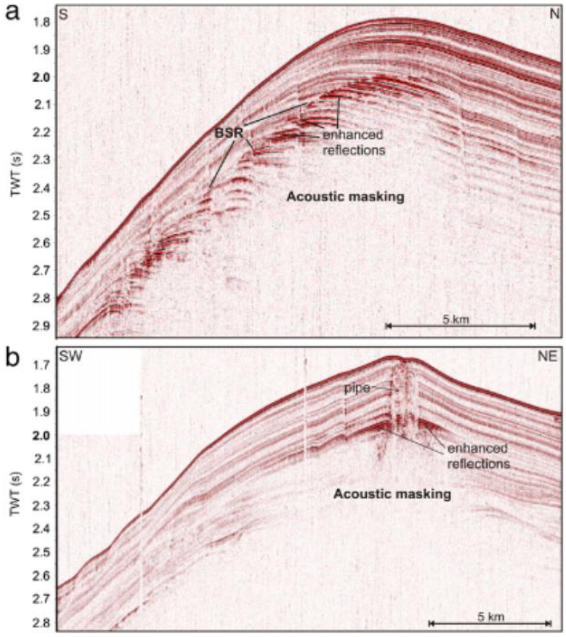

Figure 6: 2D seismic line crossing the (a) western and (b) eastern part of the ridge, showing the BSR and the free gas zone underneath. Note the chimney structure terminating in a pockmark depression in (b). From Bünz et al. (2012).

Pockmarks, depressions on the seafloor, are fluid flow structures indicating the release of free gas from the seabed (Bünz *et al*. 2012). At least six pockmarks exhibiting active methane release have been discovered along the eastern part of Vestnesa Ridge (Panieri *et al*. 2017). Pockmarks are underlain by chimneys, pipe-like channels serving as conduits for free gas to migrate through the gas hydrate stability zone (GHSZ), through a network of tectonically sensitive fractures and faults (Bünz *et al*. 2012; Plaza-Faverola *et al*. 2015). Pockmarks are concentrated along the crest of the ridge, and the absence of such features along the flanks indicates a topographical control, with lateral migration of free gas along the base of the low-permeability GHSZ and accumulation at the anticline (Bünz *et al*. 2012).

The GHSZ is marked by a bottom-simulating reflector (BSR) (Fig. 6), a result of the high contrast in acoustic impedance between the gas hydrate-saturated sediments above and the free gas reservoir below, a common sight at gas hydrate provinces at continental margins (Haacke *et al*. 2007**)**. The BSR is prominent across the region at depths between 200-250 ms TWT (Figure 6). Underlying the BSR is a thick layer of high-amplitude reflections, indicating ample amounts of free gas trapped underneath (Bünz *et al*. 2012).

Vestnesa Ridge consists of a 40 km long eastern and a ~60 km long western segment (Vogt *et al*. 1994). Sediment thickness varies from up to 5 km at the eastern segment to a few hundred of meters towards Knipovich Ridge in the south **(**Bünz *et al*. 2012).

Of the two segments, only the eastern exhibits evidence of active seepage, with bubble streams observable in the water column on echograms obtained from single-beam echo sounding (Bünz *et al*. 2012) (Fig. 7). The inactive pockmarks at the western segment also differ in morphology from their eastern counterparts, with a much smoother surface morphology, likely due to the draping of recent sediments (Bünz *et al*. 2012). Comparisons of associated chimney morphology and distribution also reveal differences, likely indicating different stress fields and related fault activation between the two segments as an explanation for differences in seep activity (Plaza-Faverola *et al*. 2015).

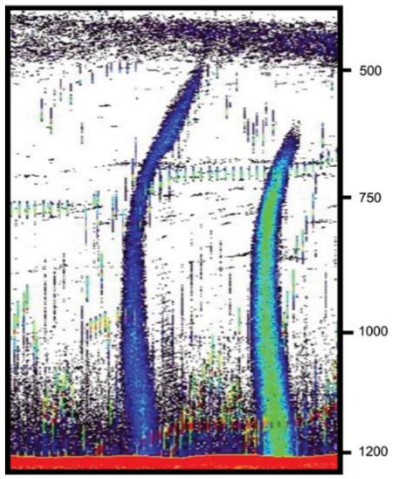

Figure 7: Bubble streams emitting from active seeps, imaged as acoustic flares in an echogram. From Bünz et al. 2012.

On the eastern segment of the ridge, two of the most active pockmarks are known as Lunde and Lomvi (Dessandier *et al*. 2019). These pockmarks are semicircular, up to 700 m across and up to 10 m deep (Panieri *et al*. 2017). Bubble streams emanate from smaller features within the pockmarks, depressions or pits with a radius of up to ~25 m. Three pits are documented in each of the 2 pockmarks (Panieri *et al*. 2017). Across the pits are ridges and blocks of methane-derived authigenic carbonates (MDAC), and findings of gas hydrates in the surface layer place the pockmarks within the GHSZ (Panieri *et al*. 2017). These pits suggest a focused, advective methane flow regime. Microbial mats of sulphur-oxidizing

bacteria are not exclusive to the pits but are found across the pockmarks (Panieri *et al*. 2017). This suggests that besides the focused flow of methane evident by bubble streams in the pit, a more steady, diffusive flow regime is also present in the pockmarks.

2.1.1 Geochemistry of fluids at Vestnesa ridge

Using Bernard and Whiticar plots **(**Bernard *et al*. 1978; Whiticar, 1999), the source of methane released from the pockmarks have been determined to be of mixed thermogenic and biogenic origin (see Figure 8 in Panieri *et al*. 2017).

2.1.2 Benthic communities at Vestnesa Ridge

Several ecological studies have been conducted on Vestnesa Ridge pockmarks to gain an understanding of faunal response to seep activity (e.g., Panieri *et al*. 2017; Bernhard & Panieri, 2018; Dessandier *et al*. 2019**)**.

Panieri *et al*. (2017) used seafloor imagery to characterize the macrofaunal communities in and around the pockmarks. In general, macrofaunal density and diversity was found to be higher within the pockmarks than on the surrounding seafloor. Tubeworms belonging to the family *Siboglinidae*, are known to live in association with chemosynthetic bacteria **(**Fig. 3; Panieri *et al.* 2017), and found across several deep-sea chemosynthetic communities **(**Rouse, 2001). The study also observed dense communities of non-chemosynthetic organisms living on the hard substrates provided by MDAC (Panieri *et al*. 2017).

2.1.3 AKMA2 Study site

The AKMA2 expedition (11^{th} -23^{rd} May 2021) onboard the R/V Kronprins Haakon examined a cluster of five pockmarks, located at the southernmost extent of Vestnesa Ridge (Panieri *et al*. 2022) (5), 12 km north of the Molloy Transform Fault. While fluid escape structures had been recognized in 2001 (Vanneste et al, 2005), active seeping hadn't been detected until the CAGE21-5 cruise of 2021 (Plaza-Faverola, 2022). The water depth of this area is ~1400 m, making it the deepest active seep on the margin (Panieri *et al*. 2022).

Figure 5d-f show ROV-captured footage of some of the sampling sites studied in this thesis. The microbial mat is grey to black, indicating the presence of *Arcobacter spp.* and *Thiomargarita spp.*, indicating very active to less active seeps, with dynamic sulfidic conditions (See Dessandier *et al*. and references therein).

3 Methods

3.1 Sampling and sample processing

During the AKMA2 expedition, the remotely operated vehicle (ROV) Ægir6000 (Fig. 8), handled by engineers from Havforskningsinstituttet (Institute of Marine Research, IMR) and Bergen University, was employed for sampling of surface sediments. The ROV was rigged with a high-resolution camera, allowing high-precision assessment and selection of sampling areas across different sub-environments related to cold seeps, for later faunal, sedimentological, and geochemical comparisons. At each station samples were taken from (1) on-site reference, in proximity of but deemed unaffected by methane (from here on out referred to as in-ref), (2) periphery of the cold seeps, characterized by the presence of methane-sequestering tube worms and (3) cold seeps and oil leaks, characterized by the presence of mats of microbial communities, methane-derived authigenic carbonates (MDAC), grazing gastropods and bubbling of methane and petroleum. Samples were collected using blade cores (32x25x10 cm) and push cores (Ø = 8 cm, length of 60 cm). Off-site reference and archive cores were using a multicorer rigged with a deep-tow camera system.

Figure 8: The ÆGIR 6000 remotely operated vehicle.

Samples were retrieved from core liners in the wet lab. Overlying water was drained from the liners using a plastic tube. For eDNA studies, ~10 g of wet sediment was collected from the very top using a sterilized plastic spoon kept in a sterilized plastic bag and fixed in LifeGuard Soil Preservation Solution. The samples were then stored at 5°C in the micropaleontology lab for the remainder of the cruise and later brought to the ID-Gene ecodiagnostics lab in Geneva for analysis.

For micropaleontological and barcoding studies, the remainder of the top 2 cm of sediment was sliced and collected in plastic cups, marked following the sample naming scheme of the

cruise. Samples were then thoroughly sieved in four fractions, 32-62 µm, 63-124 µm, 125-500 µm and 500+ µm, using stacked sieves with metallic meshes and seawater (Fig. 9).

Figure 9: Metallic mesh sieves.

Sieved samples were studied under a stereoscopic microscope. Samples were spread evenly in sorting trays wetted with seawater and cooled with freezer packs. The trays were examined one square at a time. Foraminifera were identified to genus or species level based on morphological features. When sampling for foraminifera for DNA extraction, it is important to choose live specimens. This can be ascertained based on the presence of cytoplasma and in some cases coloration. Pawlowski (2000) notes that cytoplasma can remain in the organism after DNA has started degrading, and thus the presence of pseudopoda is the best indicator. Foraminifera were picked using pipettes and tweezers, and sorted in seawater-filled petri dishes, cooled with freezer packs. Collected specimens were photographed using a camera mounted on the microscope. Organic-walled and agglutinated monothalamous specimens were stored in RNA Later buffer that preserves RNA and DNA within specimens and kept at -20°C.Textulariid and rotaliid Foraminifera were placed into micropaleontological slides and dried at ambient temperature. The remaining sediment sample was drained of water and stained using Rose Bengal in ethanol (2 g/l) for later examination and put away for storage.

Figure 4: Bottelina labyrinthica, with pen for scale.

3.2 Molecular analysis

Molecular analysis was carried out at the University of Geneva, Switzerland, in the laboratory of Maria Holzmann.

3.2.1 Scanning electron microscopy

Prior to extraction, rotaliid foraminifera assigned to different morphospecies were photographed using a JEOL JSM-65010LV scanning electron microscope (SEM) (Fig. 10a). Specimens deemed suitable, preferably larger in size, were picked using a fine brush wetted with deionized water and placed on carbon tape. Specimens were coated in gold in a vacuum chamber for 20 sec. prior to SEM imaging.

3.2.2 DNA extraction

Two different methods were employed for DNA extraction.

3.2.2.1 Guanidine extraction

Guanidine extraction method was used to isolate the DNA of small specimens. See Appendix 1 for full protocol. Guanidine extraction is a relatively quick process but does not work well for larger specimens as remaining test debris can inhibit subsequent DNA amplification. Using a fine brush or tweezers, specimens were transferred into 0,5 ml extraction tubes, containing 50 µl guanidinium isothiocyanate solution. The brush and tweezers were thoroughly rinsed in 70% ethanol and deionized water after each transfer to avoid contamination. Specimens were carefully ground using a sterilized plastic pestle and heated for 15 minutes at 60°C, using a Labnet Accublock^{TM} Digital Dry Bath incubator (Fig. 10b). Samples were then centrifuged at 8000 RPM for 1 minute in an Eppendorf 5424 centrifuge (Fig. 10b), causing debris from the test and attached sediments to form a small pellet on the bottom of the tube. 40 µl of the supernatant was then transferred to a new tube using a pipette with a sterilized filter tip. 40 µl of isopropanol was added to the solution to allow DNA precipitation, and 1 µl of GlycoBlue was added to aid the precipitation. Samples were then thoroughly mixed using a Vortex-Genie 2 vortex mixer (Fig. 10c), and left for overnight precipitation at -20°C. Following precipitation, samples were centrifuged for 20 minutes at 21000 rounds per minute (RPM), causing the DNA to form a small blue pellet at the bottom of the tube. As pellets might not always be visible, no samples were discarded based on their absence. Supernatant was removed using a pipette, and the precipitate was washed using 100 µl of a 70% ethanol solution. The samples were then centrifuged again at 21000 RPM and the

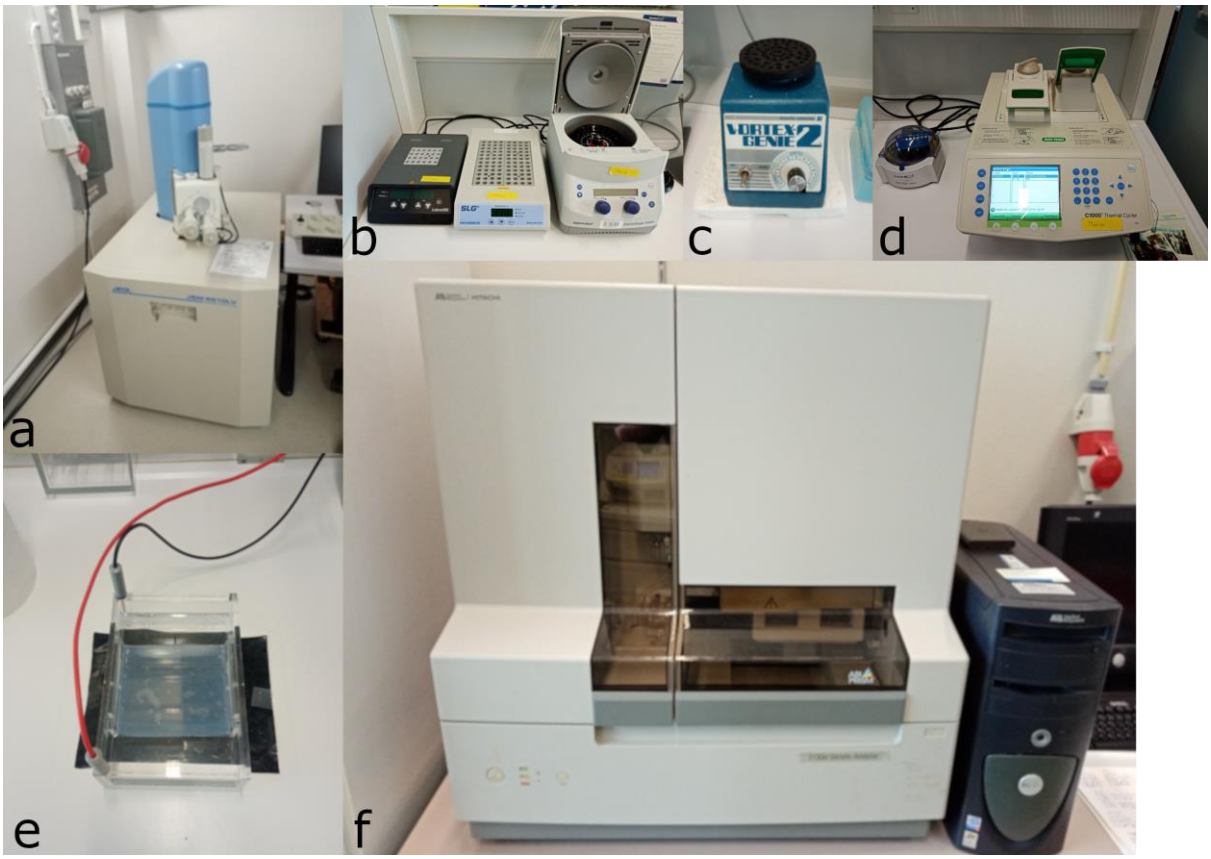

Figure 10: Lab equipment employed in the processing of samples for barcoding. a: Scanning electron microscope. b: incubators and centrifuge. c: Vortex mixer. d: Thermal cycler. e: Electrophoresis apparatus. f: Genetic analyzer.

supernatant was removed. Samples were then dried for 30 minutes at 30°C in the incubator, until all ethanol had evaporated, to prevent interference with the DNA product. 20 µl of TE buffer was added to the tubes, dissolving the pellet while keeping the DNA stable. Finally, all samples were labeled with consecutive isolate numbers and the extractions were stored at -20°C for further analysis.

3.2.2.2 DNeasy extraction

For larger specimens, such as *Bottellina labyrinthica*, the QIAGEN DNeasy^{R} Plant Mini Kit was used. See Appendix 2 for full protocol. A specimen was placed in a 1,5 ml extraction tube containing 400 µl of AP1 lysis buffer and thoroughly ground using a sterilized plastic pestle. To aid in the breakdown of proteins, 4 µl of an RNase solution was pipetted into the tube and the lysate was vortexed. The lysate was then incubated for 10 minutes at 65°C, after which 130 µl of P3 neutralization buffer was added to the tubes to precipitate proteins. After 5 minutes of incubation on ice, the product was centrifuged for 2 minutes at 21000 RPM, causing cell-debris to form a pellet at the bottom. The supernatant was transferred to a

QIAshredder mini spin column placed in a 2 ml tube and centrifuged for 2 minutes at 21000 RPM, filtering out any leftover debris. The flowthrough was transferred to 1,5 ml tubes prefilled with 675 µl of AW1 wash buffer and carefully mixed by pipetting. The solution was then transferred to a DNeasy mini spin column placed in a 2 ml tube and centrifuged for 1 minute at 8000 RPM, binding the DNA to the filter. The spin column was then placed in a new 2 ml tube and rinsed with 500 µl of wash buffer AW2 and centrifuged twice, first at 8000 RPM for 1 minute, and second, after another wash with 500 µl of AW2 buffer, at 21000 RPM for 2 minutes. Lastly, the spin column was transferred to a 1,5 ml tube, and 50 µl of elution buffer AE, preheated to 65°C, was added directly to the membrane of the spin column. The solution was incubated for 5 minutes at room temperature and then centrifuged for 1 minute at 8000 RPM for elution, causing the DNA to pass through the filter and into the collection tube. Tubes were labelled accordingly and stored at -20°C.

3.2.3 Polymerase chain reaction

The polymerase chain reaction (PCR) is a process that since its inception in 1985 (Mullis & Faloona, 1987) has revolutionized the field of molecular biology and proven a valuable tool in sectors such as diagnostics (Yang & Rothman, 2004), biomonitoring (Pawlowski *et al*. 2014), and forensics (Cavanaugh & Bathrick, 2018).

At its core, PCR utilizes a polymerase, an enzyme capable of synthesizing nucleic acids, to create many copies of a selected gene or fragment of a gene, allowing for detection and study of said gene in great detail, through sequencing (Mullis & Faloona, 1987).

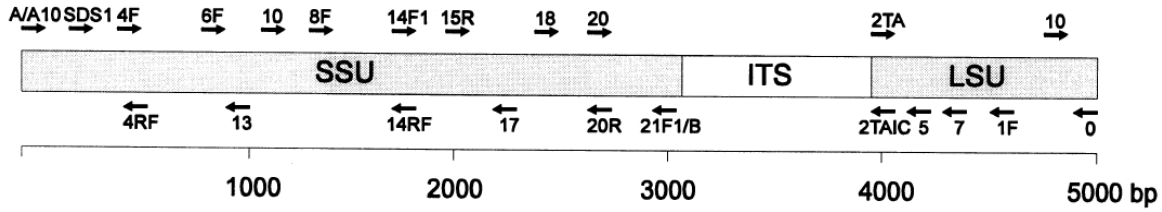

Figure 11: Diagram of sequenced rRNA genes with approximate position of primers. Source: Pawlowski, 2000.

PCR is a process in three steps, repeated for 20-40 cycles and resulting in many copies of the selected gene. The first step involves denaturation, the breakdown of the double-stranded DNA molecules into singles strands. This is done at temperatures of 90-100°C. The second step, annealing, involves the attachment of primers, short strands of oligonucleotides corresponding to each side of the target sequence, delimiting the amplified region

(Schochetman *et al*. 1988). A forward and a reverse primer is used, corresponding to both DNA strands. Figure 11 shows the positions of various primers on sequenced rRNA genes of foraminifera. The third step is the synthesis of new DNA strands, through the use of Taq polymerase. At each cycle the number of obtained copies is doubled resulting in an exponential increase of DNA molecules.

Semi-nested PCR amplification was carried out for the SSU rDNA barcoding fragment of foraminifera (Pawlowski and Holzmann, 2014) using forward primers s14F3 (acgcamgtgtgaaacttg) for the first and s14F1 (aagggcaccacaagaacgc) for the second amplification. The reverse primers s20r (gacgggcggtgtgtacaa) or sB (tgatccttctgcaggttcacctac) were used.

Thirty-five and 25 cycles were performed for the first and the second PCR, with an annealing temperature of 50°C and 52°C, respectively. The amplified PCR products were purified using the High Pure PCR Cleanup Micro Kit (Roche Diagnostics). Sequencing reactions were performed using the BigDye Terminator v3.1 Cycle Sequencing Kit (Applied Biosystems) and analyzed on a 3130XL Genetic Analyzer (Applied Biosystems).The PCR protocol can be seen in Appendix 3.

A master mix was prepared prior for each amplification in an isolated workspace (hood), to prevent contamination with extraneous DNA. The exact amounts and concentration of each of the reagents can be seen in Appendix 3. The PCR mix contains bi-distilled water, Mg-buffer, deoxynucleoside triphosphates (dNTPs), 2 primers, bovine serum albumin (BSA) and Taq polymerase. Tubes were kept on cool racks during the whole preparation. DNTPs provide the nucleotides for DNA synthesis, and BSA increases the yield of the PCR (Farell & Alexandre, 2012). The choice of primer affects the length of the studied sequence, including the number of species-specific variable regions. Refer to Table 1 in Pawlowski (2000) for a list of suitable primers, including length, sequence and specificity.

The amplification protocols can be seen in Appendix 3. One µl of extracted DNA was added to a 0,5 ml tube containing 24 ul of the prepared PCR master mix. For each run, a negative control containing the master mix but no DNA was also amplified. Amplification and subsequent re-amplification were performed using a Bio-Rad C1000^{TM} Thermal Cycler (Fig 10d). For reamplification, 1 µl of each PCR product obtained during the first amplification

was used. Initial results showed weak PCR bands, and to improve the results the amount of extracted DNA was upped to 3 µl and the number of cycles for the re-amplification was increased from 25 to 30.

3.2.4 Gel electrophoresis

Gel electrophoresis was employed to assess the quality of the PCR product and check for any possible contamination. DNA and RNA molecules, in a near-neutral pH environment, are negatively charged, and will migrate when exposed to an electrical current (Ogden & Adams, 1987). This characteristic, combined with the fact that fragments of different molecular weight migrate at different rates, can be utilized to visually discern the molecular weight (in base pairs) of the amplified fragment. The length can be gauged through comparisons with fragments of a known length (known as a ladder), and the results can be compared to the desired size of the targeted fragment (Figure 12). It is important to note that this method does not definitively identify the strand (Schochetman *et al.* 1988), and further analysis (sequencing) is required. Fragmentation of the DNA or RNA product takes place using a Tris-acetate-EDTA buffer (TAE) as the conductive medium.

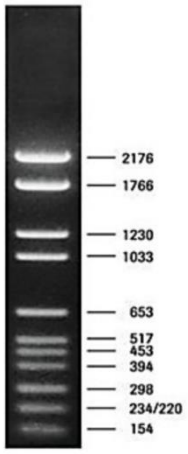

Figure 12: Fragmented ladder VI with molecular weight of fragments shown in basepairs. Source: Maria Holzmann.

Agarose gel was heated in a microwave and mixed with Sybr™ Safe DNA Gel Stain, a fluorescent dye that makes the PCR product visible in UV light. The gel was then poured into a rectangular slab cast with a comb and left to cool at room temperature. When the gel had cooled the comb was removed, leaving behind small chambers to load the PCR product into. The gel slab was placed in an electrophoresis apparatus (Fig. 6e), connected to a power supply with an anode and a cathode. 1x TAE buffer was filled into the apparatus until the gel was completely covered. 3 µl of PCR product was mixed with 1 µl of gel loading buffer. 3 µl of ladder VI with fragments of known length was loaded into the first chamber and the subsequent PCR products into the following chambers. The final chamber was filled with the negative control. A 100-volt current was run through the apparatus, creating a voltage gradient, and initiating the migration of molecules. The apparatus was left to run for roughly 30 minutes before the current was turned off. The Gel was then removed from the apparatus and placed in a GelDoc Molecular Imaging System,

capturing images of the gel for analysis. Examples of the final output can be seen in Fig. 13. Notice that DNA fragments are present in the negative control. Some contamination has likely taken place at some point during the workflow, and any results from this particular PCR run should be handled with caution or discarded. The effectiveness of the amplification can also be gauged from the apparent strength of the PCR bands. Weaker bands might suggest an increase in either the number of thermal cycles during the amplification, or an increase in DNA/RNA dose, to ensure a successful sequencing result.

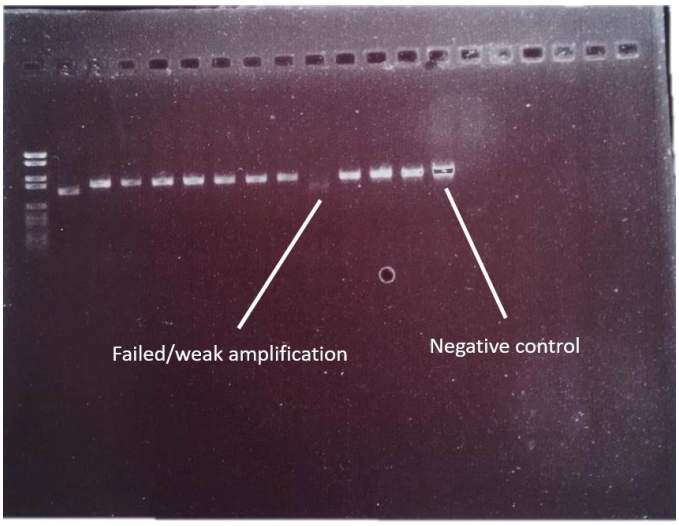

Figure 13: Output of the GelDoc Molecular Imaging System. Note the faded band indicating a weak amplification. The negative control was amplified, indicating contamination.

3.2.5 Purification

In preparation of the sequencing, the amplification product was purified using the Roche High Pure PCR Cleanup Micro Kit. The purpose of purification is to remove nucleotides, primers etc., that might hinder proper sequencing.

The amplification product was diluted with 80 µl of double distilled water and transferred into 1,5 ml tubes containing 400 µl of binding buffer and mixed through vortexing. The combined solution was then transferred to a spin column and centrifuged for 1 minute at 8000 RPM, binding the amplification product to the filter. Supernatant was removed from the collection tube and 400 µl of wash buffer was added to the spin column, removing traces of protein and primers. This step was repeated, this time with 300 µl of wash buffer. The empty spin column was then centrifuged at 21000 RPM, removing any leftover wash buffer. The spin column was transferred to a new 1,5 ml tube and 20 µl of elution buffer was added, allowing passage of the purified PCR product through the filter. After centrifuging at 8000 RPM for 1 minute, the spin column was removed and the purified product was stored at -20°C.

3.2.6 Sanger sequencing

Sanger sequencing was amongst the first generation of sequencing methods, developed in 1977 (Sanger *et al*. 1977), and combines the PCR with electrophoresis. While next-generation sequencing methods have gradually overtaken the field, Sanger sequencing still proves viable in sequencing of shorter fragments at a low cost (Totomoch-Serra *et al*. 2017). The sequencing was performed using an Applied Biosystems^{R} 3130xl Genetic Analyzer (Fig. 6f).

3.3 Morphological studies

The sediment-ethanol mixture was spread on a petri dish and examined under a Leica Z16 APO compound microscope, mounted with a Leica DMC 4500 camera. For each sample, the first ~200 Rose Bengal-stained (live-collected) specimens were identified to the highest possible taxonomic rank. Only complete tests were considered as part of the live assemblage.

Select specimens were micrographed utilizing the LAS X Z-stacking tool for documentation and as reference for further identification. When possible, specimens were identified to species or genus-level, and otherwise into "working" morphospecies, here defined as non-named morphology-based species appearing in the literature (e.g. Psammosphaerid sp. 1, as seen in Sabbatini *et al*. 2013).

The 63-125 µm size fraction was selected as it represented the most complete dataset after picking of foraminifera for barcoding studies. This size fraction has also been recommended in the literature for diversity studies of benthic foraminifera as it captures a higher diversity, especially with regards to ecologically sensitive species (Schönfeld *et al.* 2012; Dessandier *et al*. 2019), though it is unclear whether this applies to studies of soft-shelled monothalamous foraminifera as well.

Monothalamous specimens were further grouped into three larger informal groups based on test morphology, as seen in Gooday (1986, 2002) and Sabbatini *et al*. (2007, 2013). These morphogroups include allogromiids with an unambiguous organic test wall, saccamminids with a test composed of fine agglutinated particles overlying the organic test wall and distinct aperture(s), and psammosphaerids with agglutinated tests but no distinct aperture. Although lacking phylogenetic evidence, these groupings allow for informal categorizing of monothalamous communities, often comprising of undescribed taxa (Sabbatini *et al.* 2013;

Goineau & Gooday, 2017). Note that the informal grouping allogromiid is not to be confused with *Allogromiid spp.* and associated species.

Select diversity indices were calculated from the abundance data using PRIMER software (v.7), including the number of taxa, the Shannon-Wiener index (H'$\log_e$), Fisher's alpha index (α), the Pielou index (J') and Simpson's index of diversity (1-D). H' and α are both measures of diversity, while J' emphasizes the evenness in distribution of species and 1-D is the probability that two randomly selected specimens belong to different morphospecies.

4 Dataset

An overview of the cores examined in this thesis can be seen in Table 1. The cores represent all previously mentioned microhabitats (Fig. 3), with the transition from microbial mat to tubeworm zone to in-ref to reference site representing a gradient of distance away from the highest CH_4 flux. Refer to Appendix 4 for a list of all counted specimens.

Table 1: Overview of sediment cores sampled in this study.

Station	Sample code	Sampling method	ROV dive no.	Latitude	Longitude	Water depth (m)	Microhabitat	Purpose
Vestnesa Ridge	CAGE22-KH03-MUC1	Multicore	N/A	7843.31 64 N	0701.93 21 E	1380	Off-site reference	Barcoding, picking
Vestnesa Ridge	CAGE22-KH03-BC1	Bladecore	5	7842.06 60 N	0700.79 30 E	1390	Tubeworm zone	Barcoding
Vestnesa Ridge	CAGE22-KH03-PC8	Pushcore	7	7842.04 74 N	0701.04 00 E	1400	Reference in pockmark	Barcoding, picking
Vestnesa Ridge	CAGE22-KHO3-BC6	Bladecore	8	7842.07 62 N	0700.90 31 E	1397	Tubeworm zone	Barcoding, picking
Vestnesa Ridge	CAGE22-KH03-PC15	Bladecore	13	7842.05 33 N	0700.85 04 E	1391	Microbial mat	Picking

An overview of all sequenced specimens can be seen in table 2. Of the 25 Sequenced specimens, sequences were successfully obtained from 13 specimens, upon inspection assigned to the morphospecies *Bolivina pseudopunctata* (Höglund, 1947), *Stainforthia fusiformis* (Williamson, 1858) and *Epistominella exigua* (Brady, 1884). 11 of the specimens obtained extraneous sequences, belonging to *Lacogromia sp.*, two unknown Rotaliid sequences and *Stainforthia sp*. From one specimen, no sequences were obtained.

Table 2: Overview of all sequenced specimens.

Isolate no.	Morphospecies	Sample code	Primers	Extraneous sequence
21585	*Bolivina pseudopunctata*	KH03-BC3	14F1-sB	*Lacogromia sp.*
21588	*Stainforthia fusiformis*	KH03-BC6	14F1-sB	
21589	*Stainforthia fusiformis*	KH03-BC6	14F1-sB	
21591	*Stainforthia fusiformis*	KH03-MUC1	14F1-sB	
21592	*Stainforthia fusiformis*	KH03-MUC1	14F1-sB	
21597	*Stainforthia fusiformis*	KH03-PC8	14F1-sB	
21601	*Stainforthia fusiformis*	KH03-MUC1	14F1-sB	
21602	*Stainforthia fusiformis*	KH03-PC2	14F1-sB	Unknown Rotaliid
21603	*Epistominella exigua*	KH03-MUC1	14F1-sB	
21604	*Epistominella exigua*	KH03-MUC1	14F1-sB	
21605	*Epistominella exigua*	KH03-MUC1	14F1-sB	
21606	*Epistominella exigua*	KH03-MUC1	14F1-sB	
21558	Small miliolid	KH03-MUC1	14F1-s20r	*Lacogromia sp.*
21559	small miliolid	KH03-MUC1	14F1-s20r	*Lacogromia sp.*
21561	small miliolid	KH03-MUC1	14F1-s20r	*Lacogromia sp.*
21539	*Bolivina pseudopunctata*	KH03-BC1	14F1-s20r	
21540	*Bolivina pseudopunctata*	KH03-BC1	14F1-s20r	
21547	*Bolivina pseudopunctata*	KH03-BC1	14F1-s20r	
21605	*Epistominella exigua*	KH03-MUC1	14F1-s20r	No sequence obtained
21608	*Pyrgo sp.*	KH03-MUC1	14F1-s20r	Unknown Rotaliid
21611	*Pyrgo sp.*	KH03-MUC1	14F1-s20r	*Stainforthia sp.*
21612	*Bottellina labyrinthica*	KH03-MUC1	14F1-s20r	*Lacogromia sp.*
21613	*Bottellina labyrinthica*	KH03-MUC1	14F1-s20r	*Stainforthia sp.*
21614	*Bottellina labyrinthica*	KH03-MUC1	14F1-s20r	*Stainforthia sp.*
21615	*Bottellina labyrinthica*	KH03-MUC1	14F1-s20r	*Stainforthia sp.*

4.1 Limitations to the dataset

The dataset obtained for this study was originally sampled and processed for the purpose of single-cell DNA extraction and barcoding of foraminifera. A large number of foraminifera were removed without regard for species counting.

This processing hinders meaningful numerical and statistical studies of abundance for most of the samples collected. For a handful of samples, the picking of foraminifera for barcoding was almost exclusively targeted at calcareous foraminifera. Rose Bengal staining and subsequent examination revealed an abundance of stained (live-collected) soft-shelled forms. Thus, while caution should be taken in assessing the ecological status of foraminifera across microhabitats based on this dataset, it might at least provide semi-quantitative comparisons of relative

abundance of select soft-shelled foraminifera, given that a sample size of ~200 specimens reflect larger trends in ecology.

5 Results

5.1 Scanning electron microscopy

All sequenced specimens can be seen in Plate 1.

5.1.1 Stainforthia cf. fusiformis

The overall test shape is elongated and fusiform (Fig. 14). Test length ranges between 165 and 318 µm, with an average length of 260 µm (n = 20). The widths range between 78 and 162 µm, with an average of 101 µm. The length:width ratio ranges from 2,0 to 3,9 with an average of 2,7. The chambers are arranged in a biserial manner, inflated, elongated, and overlap each other, increasing in size towards the apertural end. The micrographed specimens have 5-10 chambers, with an average of 7,1**.** The aperture is usually well-defined as a large depression at the base of the final chamber, though sometimes covered in debris (Fig. 14b). Pores are tiny and scattered, usually concentrated more towards the prolocular end of the chamber (Fig. 14c). Sutures are well-defined with a slight depression. The proloculus is spherical.

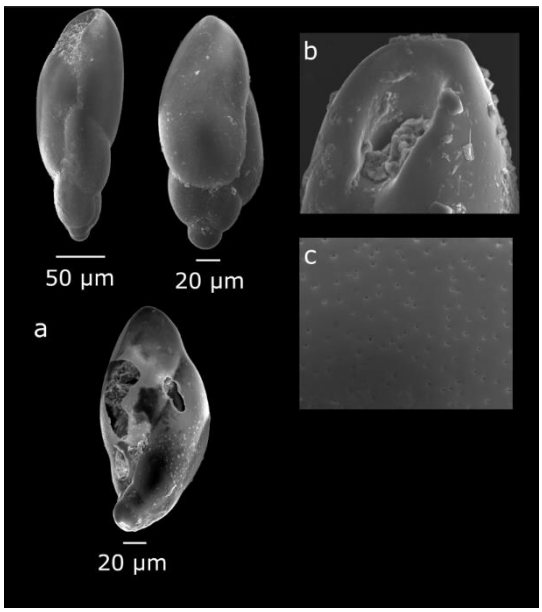

Figure 14: Scanning electron micrographs of Stainforthia cf. fusiformis. a: Three of the specimens that sequenced (Isolate no. 21588, 21589, 21592). b: Close-up of aperture. c: Close-up of pores.

Sequences were obtained from a total of six specimens (Plate 1).

5.1.2 Bolivina pseudopunctata

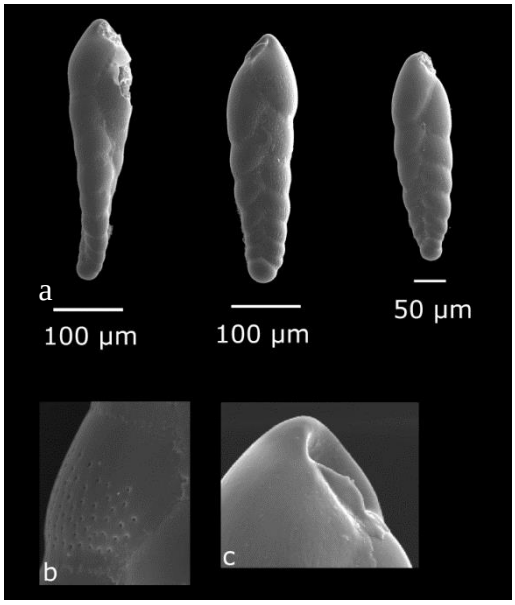

Figure 15: Scanning electron micrographs of B. pseudopunctata. a: The three specimens that sequenced. b: Close-up of pores and ragged sutures. c: Close-up of aperture showing toothplate.

The overall test shape is elongated and approximately coniform, with a torsion more pronounced in some specimens than others (Fig. 15). Test length ranges between 241 and 443 µm, with an average of 324 µm (n = 17). The torsion of the test prevented correct measurements of width. The chambers are arranged in a biserial manner, inflated and subcircular to elongated, with an increasing elongation towards the apertural end and a strong overlap. The micrographed specimens have 13-16 chambers, with an average of 14,6. Pores are relatively large and concentrated towards the half of the chamber closest to the proloculus (Fig. 15b). Sutures vary slightly, with some being well-defined and smooth depressions, others less defined, and some being more ragged in character (Fig 15b). The proloculus is spherical. Aperture is well-defined where visible, as a depression at the base of the final chamber, with a straight to semi-curved toothplate (Fig. 15c).

Sequences were successfully obtained from a total of three specimens.

5.1.3 Epistominella exigua

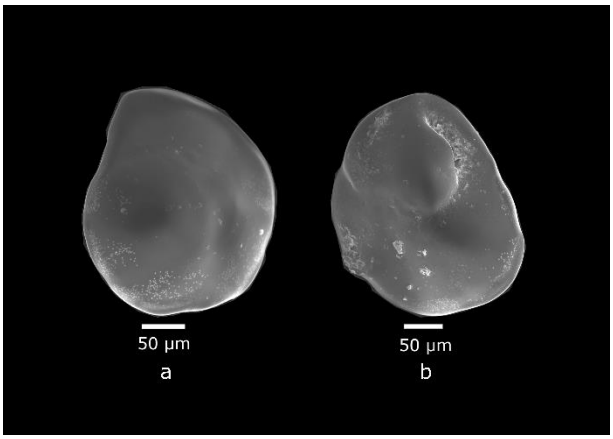

Figure 16: Scanning electron micrographs of E. epistominella. a: Umbilical view. b: Aperturial view.

The test is subcircular to circular, with the chambers arranged in a low trochospiral coil (Fig. 16). Test diameter range between 243 and 277 µm, with an average of 265,5 µm (n = 4). The exact number of chambers is hard to distinguish due to the not very well-defined sutures. The test is smooth around the proloculus, with tiny pores concentrated around the periphery of the test. The aperture is covered by a curved toothplate (Fig. 16b).

Sequences were successfully obtained from a total of four specimens.

5.1.4 Milliolida

The unidentified miliolid has an elongated, fusiform, smooth test, (Fig. 17). Three tubular chambers are distinguishable on the photographed specimens, with the apertural chamber overlapping the others. The specimens vary in length between 183 and 211 µm, with an average of 199,5 (n = 4). The width ranges between 83 and 92 µm, with an average of 86,8 µm. The length:width ratio ranges from 2,2 to 2,4 with an average of 2,3. The most striking feature is the thick calcareous rim observed around the aperture. While the chamber arrangement is

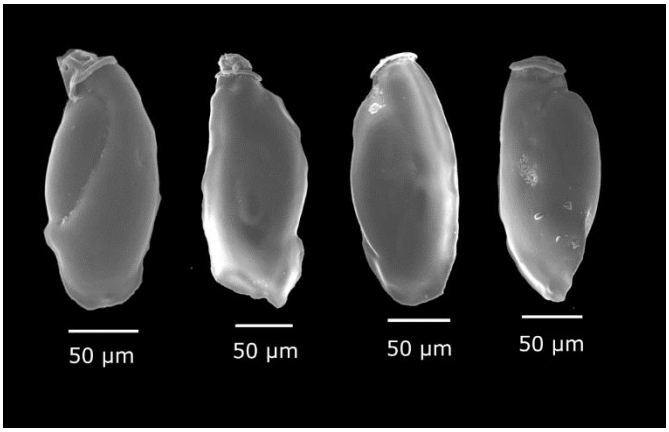

Figure 17: Scanning electron micrographs of four millolid specimens belonging to the same morphotype.

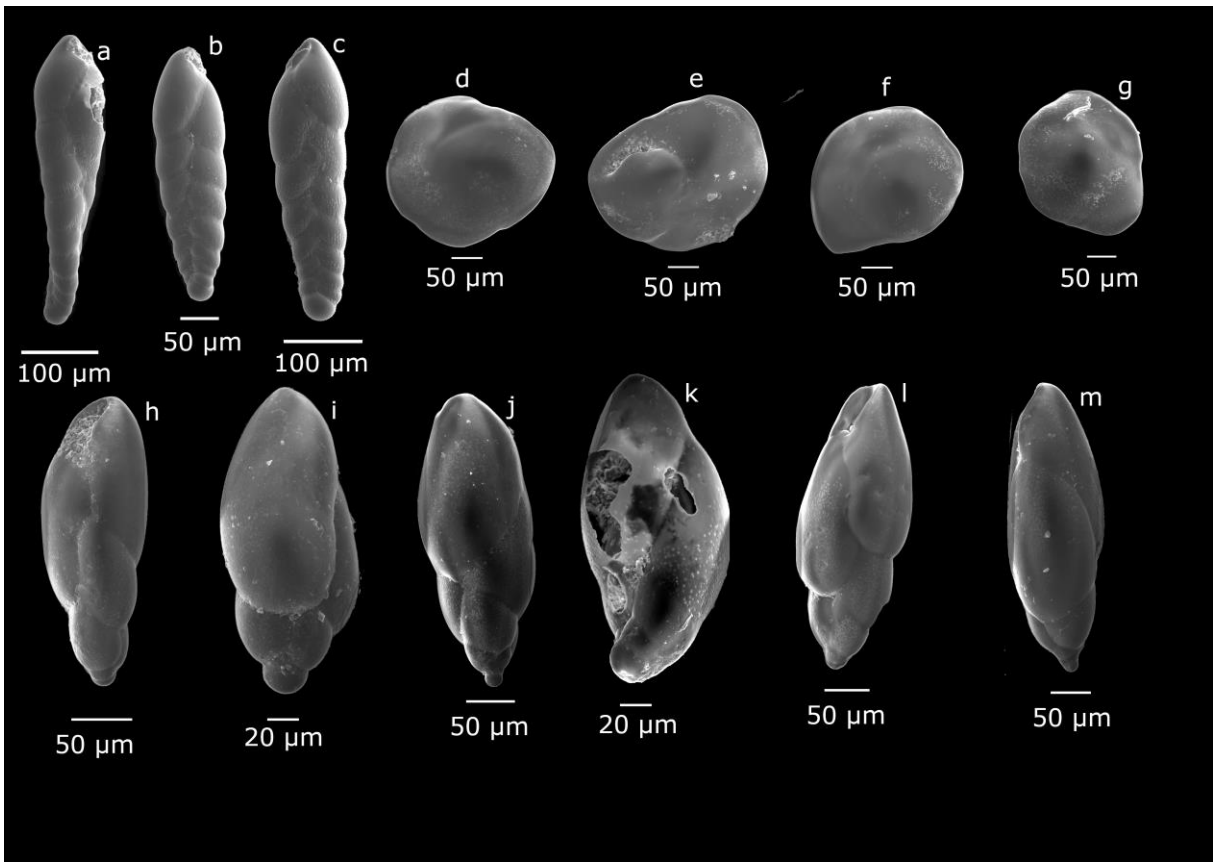

Plate 1: Scanning electron micrographs of all sequenced specimens. a-c: Bolivina pseudopunctata. d-g: Epistominella exigua. h-m: Stainforthia cf. fusiformis.

similar to that of *Miliolina oblonga* (Montagu, 1803), the calcareous rim and overall chamber arrangement is most similar to a species named *Spirophthalmidium acutimem?*, though no more information is available on this species, outside of a book (Haywards & Ryland, 1990), that is not available online.

None of the miliolida successfully sequenced.

5.2 Phylogenetic analyses

All phylogenetic trees were constructed using comparable sequences (>84 % identical for *B. pseudopunctata*, >95 % identical for *Stainforthia cf. fusiformis.*, > 95 % identical for *E. exigua*, outgroup taxa excluded) obtained from the publicly available 18S database of foraminifera (NCBI; https://www.ncbi.nlm.nih.gov/nucleotide/), using the Basic Local Alignment Search Tool (BLAST). Sequences were aligned in SeaView v. 4.4.3 (Guoy *et al*. 2010), using the muscle alignment option. Maximum likelihood phylogenies were constructed using PhyML 3.0 (Guindon *et al*. 2010**)**. Suitable substitution models were automatically selected using Smart Model Selection (LeFort *et al*. 2017), based on Akaike Information Criterion, resulting in a GTR+R model being used for *B. pseudopunctata*, a TN93+R model being used for *Stainforthia cf. fusiformis*, and a GTR+G model being used for *E. exigua* . Starting trees are based on the BioNJ algorithm (Gascuel, 1997). Standard bootstrap analyses were performed with 100 replicates.

Table 3: Overview of all newly obtained sequences used in this study, including assigned morphospecies, isolate numbers, sampling locality and water depth, primers used and sampling microhabitat.

Species	Isolate no.	Sampling locality	Water depth (m)	Primers	Microhabitat
Bolivina pseudopunctata	21539	Vestnesa Ridge	1390	14F1-s20r	Tubeworm zone
Bolivina pseudopunctata	21540	Vestnesa Ridge	1390	14F1-s20r	Tubeworm zone
Bolivina pseudopunctata	21547	Vestnesa Ridge	1390	14F1-s20r	Tubeworm zone
Epistominella exigua	21603	Vestnesa Ridge	1380	14F1-sB	Reference
Epistominella exigua	21604	Vestnesa Ridge	1380	14F1-sB	Reference
Epistominella exigua	21605	Vestnesa Ridge	1380	14F1-sB	Reference
Epistominella exigua	21606	Vestnesa Ridge	1380	14F1-sB	Reference
Stainforthia cf. fusiformis	21588	Vestnesa Ridge	1397	14F1-sB	Tubeworm zone
Stainforthia cf. fusiformis	21589	Vestnesa Ridge	1397	14F1-sB	Tubeworm zone
Stainforthia cf. fusiformis	21591	Vestnesa Ridge	1380	14F1-sB	Reference
Stainforthia cf. fusiformis	21592	Vestnesa Ridge	1380	14F1-sB	Reference
Stainforthia cf. fusiformis	21597	Vestnesa Ridge	1400	14F1-sB	In-site reference
Stainforthia cf. fusiformis	21601	Vestnesa Ridge	1380	14F1-sB	Reference

For an overview of all newly obtained sequences used in this study, refer to Table 3. Refer to Appendix 5 for an overview of all sequences used for phylogenetic analysis in this thesis, including accession numbers, sampling locality, and water depth at sampling locality where available.

5.2.1 Epistominella exigua

SSU rDNA sequences obtained from four specimens assigned to the morphospecies *E. exigua* sampled from the Vestnesa Ridge reference site (water depth = 1380 m) were compared to 18 sequences belonging to the *Epistominella* genus (Fig 18).

The 18 sequences include nine *E. exigua* collected at varying water depths in the Weddell Sea (AM491306, AM491307, DQ195557, HE998671), Pacific Ocean (FJ185800, FJ185805, FJ185806) and the Northern Atlantic Ocean (LN873804, LN873805), three *Epistominella sp. 1* from King George Island, Antarctica (FJ185807, FJ185808, FJ185812), two *Epistominella sp. 2* from King George Island (FJ185813, FJ185817), one *Epistominella sp. 3* from the Pacific Ocean (FJ185820) and four *E. vitrea* (Parker, 1953) from McMurdo Sound, Antarctica (AM491308, AM491312), Weddell Sea (AM491311) and Ushuaia, Argentina (LN873812). The textulariids *Trochammina hadai* (Uchio, 1962) (MZ707234) and *T. inflata* (Montagu, 1808) (MZ707245) were selected as outgroup taxa.

Phylogenetic analysis reveals three major groups with further branching into several subgroups (Fig. 5). Group 1 comprises all sequences of *E. exigua* as well as *Epistominella sp. 2* (depths 20-100 m) and *3* (depth 1110 m). The well-supported (BV = 90) sister group comprises *E. vitrea* (depths 0-1200 m) and *Epistominella sp. 1* (depths ~100 m). The outgroup branches off at the base of the tree, comprising the 2 outgroup taxa *T. hadai* and *T. inflata*.

All *E. exigua* are grouped closely together, with little to no genetic diversity (Fig. 5), scale is given as 0,02 substitutions per site). Four *E. exigua* sampled from depths deeper than 4650 m (AM491306, AM491307, DQ195557, HE998671, LeCroq *et al*. 2009) differ slightly from the rest of the *E. exigua*, and *Epistominella sp. 2* and *3* branch off in a subgroup, although this relationship is poorly resolved (BV < 50).

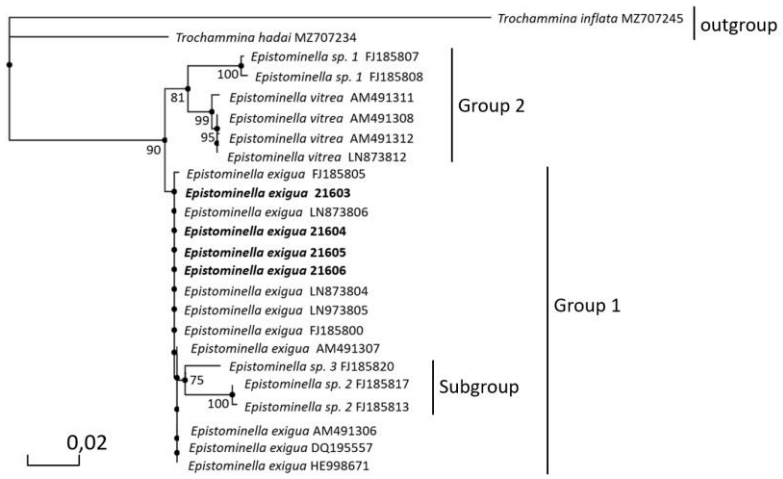

Figure 18: Maximum likelihood tree of the 18S gene of E. exigua. Bootstrap values ≥50% under maximum likelihood are shown at nodes. Scale is given at substitutions per site. Newly obtained sequences are shown in bolded letters with isolate numbers. Sequences from the BLAST database are shown with assigned species followed by accession number.

The sister group, group 2, is well resolved at all internal branches with all BV > 80 (Fig. 5) and shows the internal relations between the shallow water species *E. vitrea* and *Epistominella sp. 1*.

5.2.2 Bolivina pseudopunctata

SSU rDNA sequences of three specimens assigned to the morphospecies *B. pseudopunctata* collected from the tubeworm zone at Vestnesa Ridge (water depth = 1390) were compared to 13 sequences, mostly belonging to the genus *Bolivina* (Fig. 19).

The 13 sequences include one *B. pseudopunctata* from Gullmar Fjord, Sweden (ON818347), one undetermined foraminiferan sp. N10 from the Atlantic Ocean off-shore Namibia (FM999849), three *B. subaerenensis* (Cushman, 1922b) from the Eastern Pacific Ocean (AY465838, AY465839, AY465840), one *B. argentea* (Cushman, 1926) from the Santa Barbara Basin, off the American west coast (JQ013745) two *B. cacozela* (Vella, 1957) from New Zealand (LN886734, LN886737), two *Bolivina sp.* from New Zealand (LN 886738, LN886739), and for the outgroup taxa two *Trifarina earlandi* (Parr, 1950) (LN873502, MG980241) and one *Liebusella goesi* (Höglund, 1947) (FR754402) were selected.

Phylogenetic analysis reveals three well-resolved groups (Fig. 19). Group 1 comprises the three new sequences, with the only other *B. pseudopunctata* being the closest relative (although this subgroup is poorly resolved) and the unidentified foraminiferan sp. N10 from

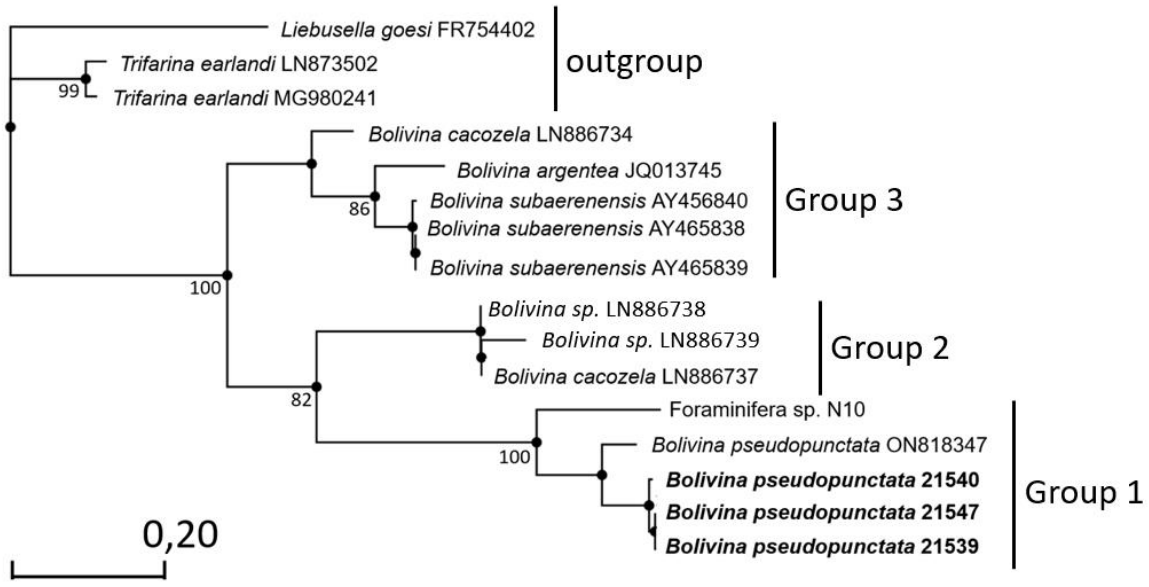

Figure 19: Maximum likelihood tree of the 18S gene for B. pseudopunctata. Bootstrap values ≥50% under maximum likelihood are shown at nodes. Scale is given at substitutions per site. Newly obtained sequences are shown in bolded letters with isolate numbers. Sequences from the BLAST database are shown with assigned species followed by accession number.

the Southern Atlantic Ocean branching off. Some genetic variation is observed within the three new sequences, as isolates no. 21539 and 21547 appear to be closer related than with sequence no. 21540, although the divergence is very low (scale given at 0,20 substitutions per site. Group 2 comprises the two *Bolivina sp.* and one *B. cacozela* from New Zealand. Group 3 comprises the three *B. subaerenensis* (water depth = 779 m) as well as *B. argentea* (water depth = 430 m) and *B. cacozela* at the base.

5.2.3 Stainforthia cf. fusiformis

SSU rDNA sequences of six specimens morphologically similar to the morphospecies *S. fusiformis* sampled from the outside reference area (21591, 21592, 215601), the in-ref (21597) and the tubeworm zone (21588, 21589) were compared to 18 sequences, mostly belonging to the genus *Stainforthia* (Fig. 20)

The 18 sequences include six *S. fusiformis* sampled from Skagerrak, Sweden (AY934744, HE998670), Dunstaffnage, Scotland (AY934745), Sweden (HG425204), Ushuaia, Argentina (LN873863, LN873864, LN873865), and Tierra Del Fuego, Argentina (L873869), eight undetermined *Stainforthia sp.* from the Beagle Strait, Chile (MG980245, MG980248, MG980249, MG980252, MG980253), Admiralty Bay, Antarctica (MG980243) Svalbard

(AY934743) and Ushuaia, Argentina (LN873866), one *Fursenkoina complanata* (Egger, 1893) from Gullmar Fjord, Sweden (ON818446), included for its morphological similarities, and for the outgroup *T. hadai* (MZ707234) was chosen. The final sequence included, ASV4, is an amplicon sequence variant (ASV) belonging to a *Stainforthia sp.*, obtained from metabarcoding of sediments across all micro-habitats in Vestnesa Ridge. This sequence is shorter with 120 bp, and only comprises the hypervariable region 37f.

Phylogenetic analysis reveals two groups (Fig 20). Group 1 comprises all *S. fusiformis* sequences obtained for this study, comprising a moderately supported subgroup at BV = 77, and displaying a high degree of genetic homogeneity across all micro-habitats, most closely related with shallow-water specimens (water depth = 44 m) of *Stainforthia sp.* from Chile and one specimen of *S. fusiformis* from unknown water depths at Tierra del Fuego. Further out in this grouping is a *Stainforthia sp.* sequence from Svalbard and a *Stainforthia* sequence from an environmental sample from the Sea of Japan (water depth = 779 m). Sequences belonging to *S. fusiformis* from Dunstaffnage, Scotland and Skagerrak, Sweden, group together in a subgroup with moderate support at BV = 73. Group 2 comprises three *Stainforthia sp.* from

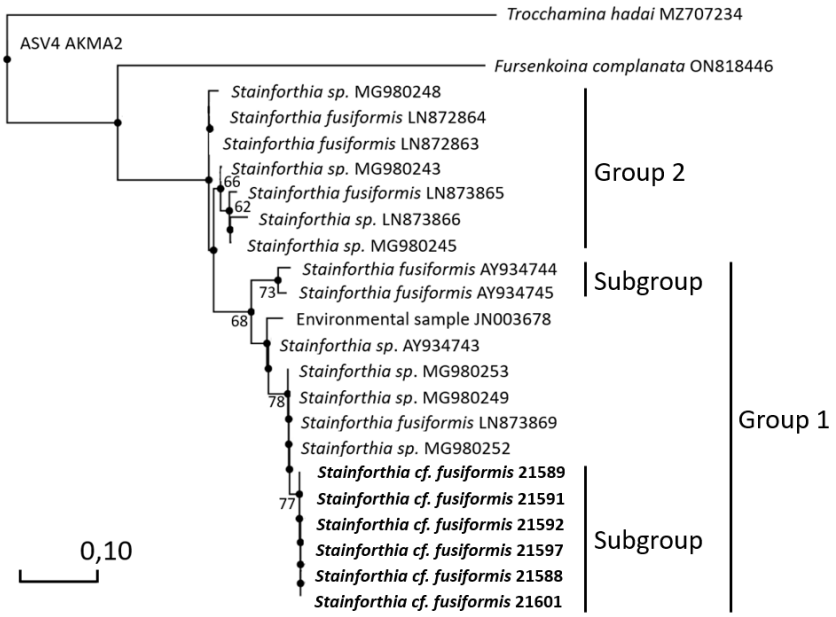

Figure 20: Maximum likelihood tree of the 18S gene from Stainforthia cf. fusiformis from reference site, in-site reference and tubeworm zone at Vestnesa Ridge. Bootstrap values ≥50% under maximum likelihood are shown at nodes. Scale is given at substitutions per site. Newly obtained sequences are shown in bolded letters with isolate numbers. Sequences from the BLAST database are shown with assigned species followed by accession numbers.

Argentina, Antarctica, and Chile, as well as one *S. fusiformis* from Argentina. The third group, of all the *Stainforthia* sequences most distantly related to the new sequences,

comprises two *S. fusiformis* from Argentina and one *Stainforthia sp.* from Chile. *Fursenkoina* complanata branches off as an outgroup to the clade comprising all *Stainforthia* sequences, and at the base of the tree the outgroup taxon *T. hadai* branches off together with the ASV.

5.3 Results of the morphological dataset

A total 801 Rose Bengal-stained specimens belonging to 56 taxonomical units were picked from the four samples. After the removal of calcareous taxa due to the aforementioned limitations to the dataset, the total number of identified specimens was 713 and of taxonomical units 39 (Fig. 21).

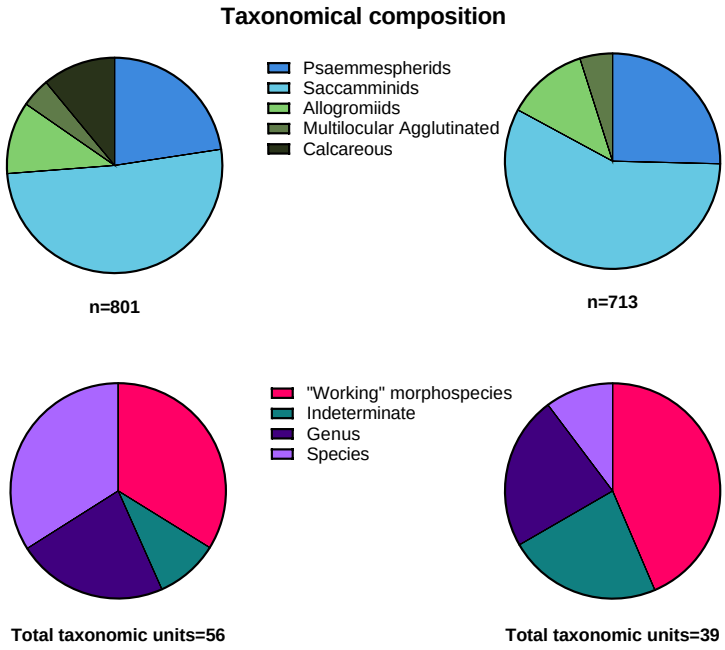

Figure 21: Overview of the taxonomical composition of the dataset before and after removal of calcareous taxa. Top: Taxonomical compostion based on informal morphological groupings. Bottom: Highest assigned taxonomical rank of the specimens in the dataset.

The sample recovered from the reference site, after removing calcareous taxa, contained 163 identified specimens belonging to 33 taxa. The sample recovered from the in-ref contained 183 specimens, belonging to 22 taxa. The sample recovered from the tubeworm zone contained 175 specimens, belonging to 33 taxa. The sample recovered from the microbial mat contained 192 specimens, belonging to 15 taxa.

A large number of various monothalamids and multilocular taxa were removed from the samples for barcoding studies prior to Rose Bengal staining. Some of these can be seen in Plate 2.

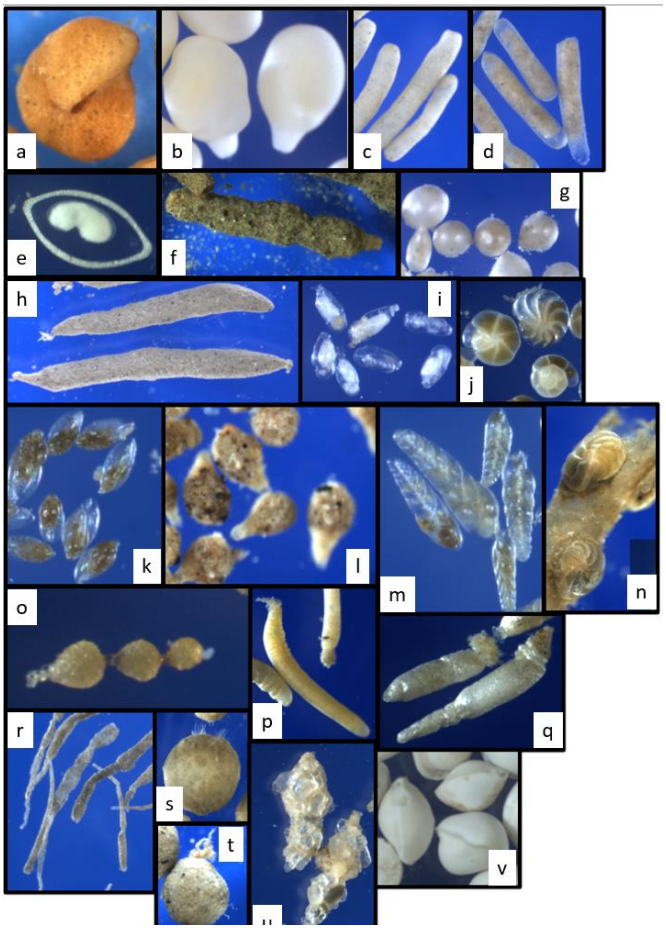

Plate 2: A selection of benthic foraminifera picked from the dataset for barcoding studies. a: Cribrostomoides crassimargo. b: White saccamminid 1. c: Hippocrepinella hirudinea. d: Uknown allogromiid. e: Vanhoeffenella sp. f: Bottelina labyrinthica. g: Phainogullmia sp. h: Pelosina variabilis. i: Undetermined miliolida. j: Cassidulina sp. k: Stainforthia fusiformis. l: Unknown saccamminid. m: Bolivina pseudopunctata. n: Cibicidoides wuellerstorfii. o: Rheophax guttifer. p: Bowseria-like. q: Unknown silver saccamminid. r: Bathysiphon sp. s: Chrithionina hispida. t: Pelosina variabilis. u: Rheophax subfusiformis. v: Pyrgo sp.

5.3.1 **Faunal composition**

For all samples, the most picked specimens are saccamminids, comprising 40% of the assemblage at the reference site, 45% at the in-ref site, 61% in the tubeworm zone and 80% in the microbial mat (Fig. 22). Psammosphaerids also constitute a significant proportion of all assemblages, with 25% at the reference site, 32% at the in-ref, 26% in the tubeworm zone and 19% in the microbial mat (Fig. 22). The allogromiids display a declining trend towards the microbial mat, with 25% at the reference site, 16% at the in-ref,

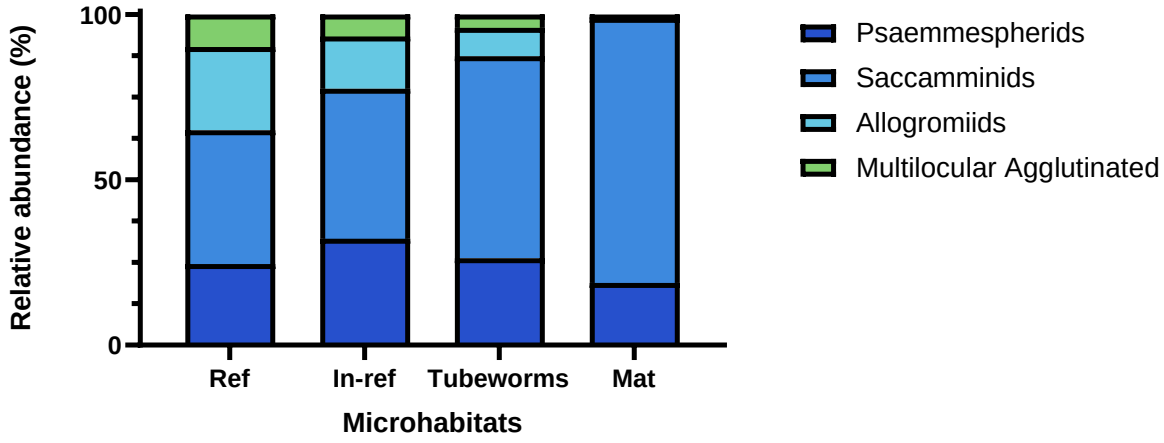

Figure 22: Relative abundance of the informal morphogroups at the different sampling microhabitats.

9% in the tubeworm zone and 1% in the microbial mat (Fig. 22). Finally, the multilocular agglutinated taxa exhibit a similar declining trend with proximity to the microbial mat, comprising 10% of the assemblage at the reference site, 6,5% at the in-ref and 4% in the tubeworm zone before disappearing completely from the assemblage in the microbial mat (Fig 22).

Select saccamminids can be seen in Fig. 23. A total of 17 saccamminid morphotypes were identified across the four samples. The number of saccamminid types at each site range between seven and 12, with the most diverse saccamminid assemblage found in the tubeworm zone.

Select psammosphaerids can be seen in Fig. 24. A total of nine psammosphaerid morphotypes were identified across the four samples. The number of psammosphaerids types at each site range between five and seven, with the most diverse psammosphaerid assemblage found in the tubeworm zone.

Figure 23: Select saccamminids. a-b: Saccamminid sp. 6. c-e: White saccamminid 1. f: Reference image of Saccamminid sp. 6 from Sabbatini et al. 2013. g: Unidentified saccamminid 2 from Majewski et al. 2005. h: White saccamminid 2. i: Saccamminid sp. 6e. j: Psammophaga sp. k: reference for Psammosphaga. Photos by Jan Pawlowski. l: Psammosphaga sp. 2. n: Saccamminid sp. 6e.

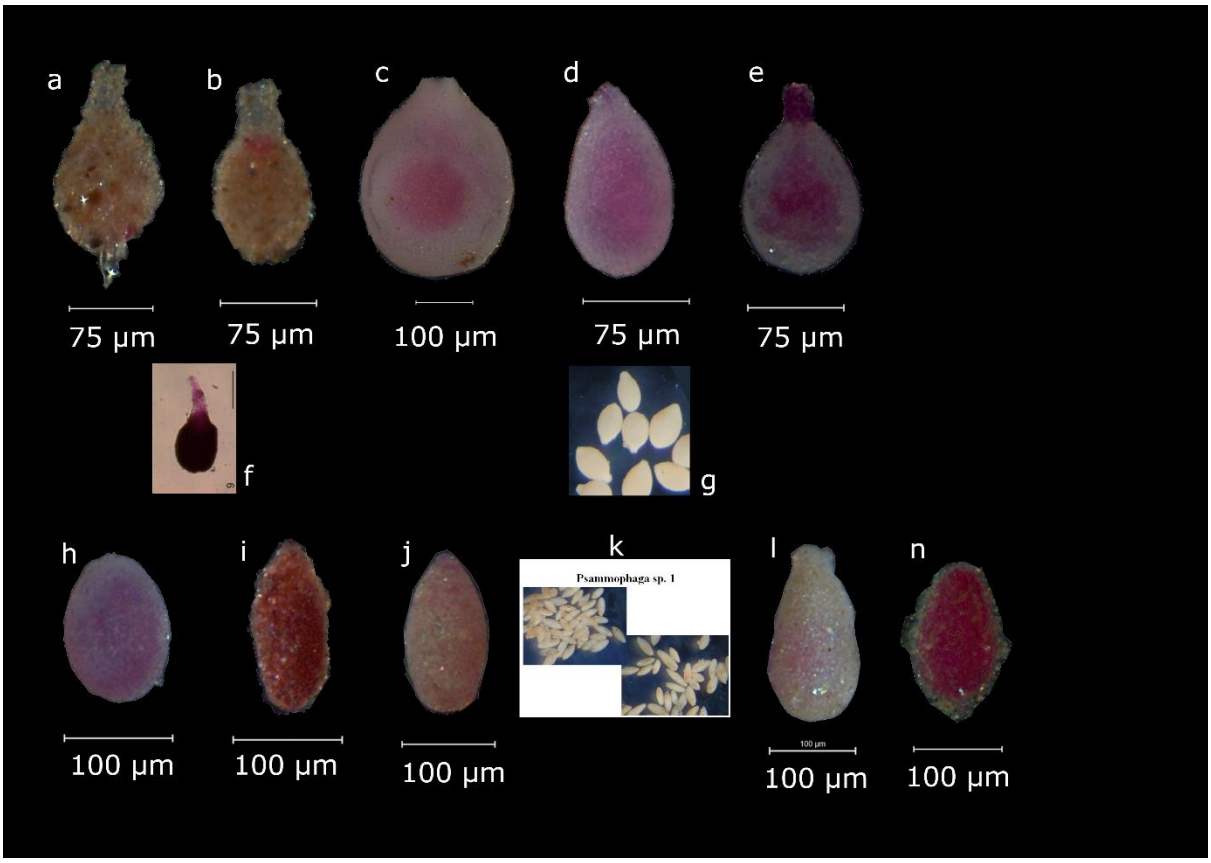

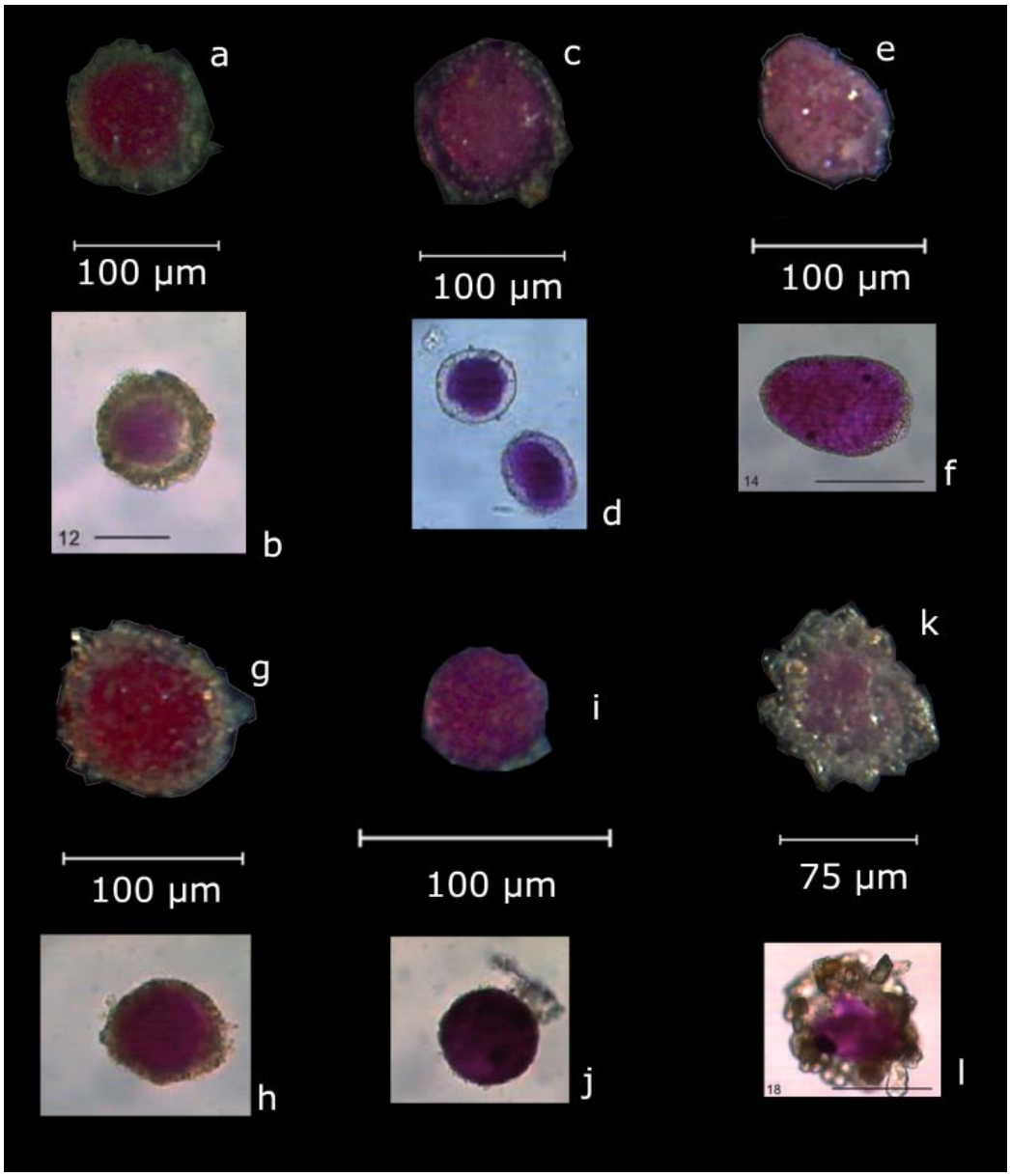

Figure 24: Psammosphaerids. a: Psammosphaerid sp. 1. b: Reference image for Psammosphaerid sp. 1. c: Psammosphaerid sp. 2. d: Reference image of Psammosphaerid sp. 2 e: Psammosphaerid sp. 3. f: Reference image of Psammosphaerid sp. 3. g: Psammosphaerid sp. 4. h: Reference image of Psammosphaerid sp. 4. i: Psammosphaerid sp. 5. j: Reference image of Psammosphaerid sp. 5. k: Psammosphaerid sp. A. l: Reference image of Psammosphaerid sp. A. All reference images sourced from Sabbatini et al. (2013)

Select allogromiids can be seen in Fig. 25. Seven morphotypes were identified across the four samples. The number of allogromiid types at each site ranges between one and four, with the fewest found in the microbial mat.

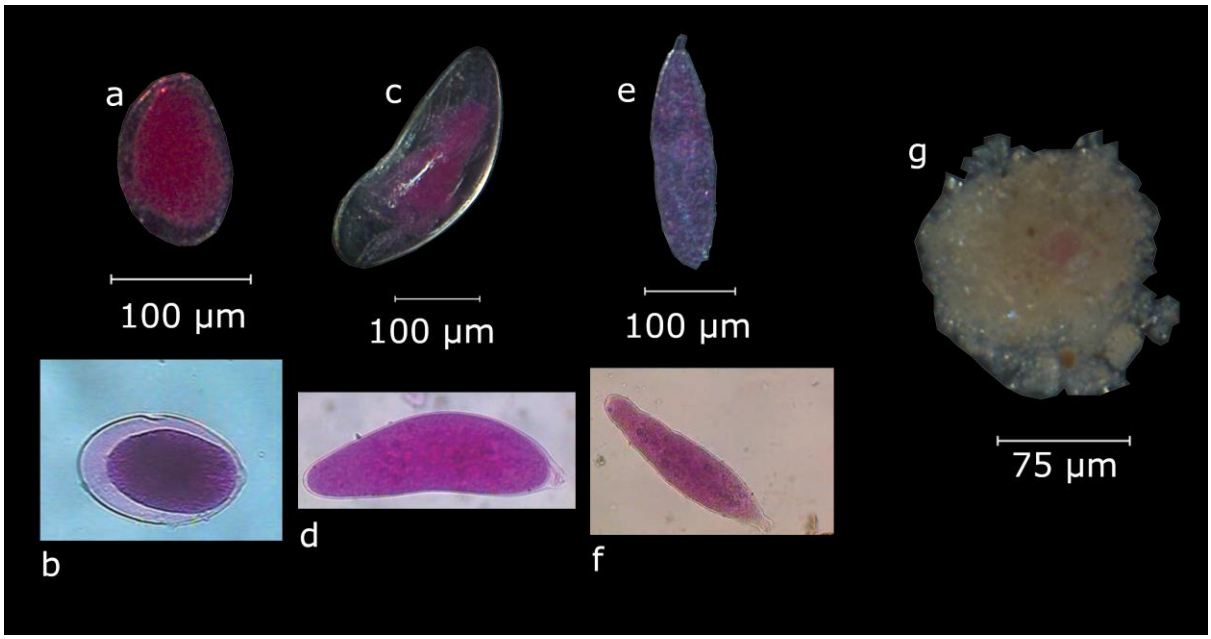

Figure 25: Select allogromiids. a: Allogromiid sp. G. b: Reference image of Allogromiid sp. G from Sabbatini et al. 2013. c: Goodayia sp. d: Reference image of Goodayia sp. from Sabbatini et al. 2013. e: Vellaria sp. f: Reference image of Vellaria sp. from Sabbatini et al. 2013. g: Mudball allogromiid.

Select multilocular agglutinated foraminifera can be seen in Fig. 26. A total of six species were identified. The number of multilocular agglutinated species at each site range between zero and five, with the most diverse assemblage being found at the reference site and no species identified in the microbial mat.

The ten most occurring species across all samples can be seen in Table 4.

Table 4: The top ten species ranked by abundance in all samples combined.

Ranked	Species	Number	% of total assemblage
1	Psammosphaerid sp. 4	71	9,96
2	Saccamminid sp. 6	65	9,12
3	Allogromiid in mudball	63	8,84
4	*Psammophaga sp.*	52	7,30
5	White saccamminid 1	48	6,73
6	Unidentified saccamminid 1	44	6,17
7	Saccamminid sp. 6e	34	4,77
8	Psammosphaerid sp. 1	33	4,63
9	Unidentified saccamminid 2	32	4,50
10	Saccamminid sp. 17	31	4,35

The most abundant species found was Psammosphaerid sp. 4 (Fig. 24g), as seen in Sabbatini *et al*. (2013), which made up ~10% of the total assemblage and was found in each microhabitat. This morphotype is monothalamous with a spherical, finely agglutinated test, comparably thinner than that of Psammosphaerid sp. 1, and comparably coarser than that of Psammosphaerid sp. 2, which has an opaquer test (Fig 24).

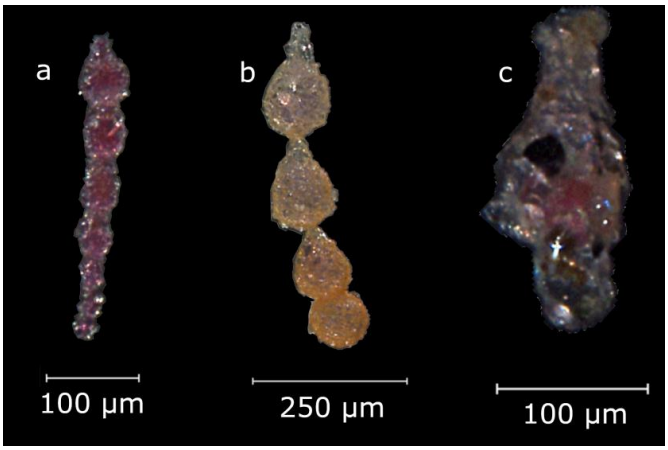

Figure 26: Select Multilocular agglutinated specimens. a: Rheophax nodulosa. b: Rheophax guttifer. c: Rheophax subfusiformis.

Saccamminid sp. 6 (Fig. 23a-b), as seen in Sabbatini *et al.* (2013) was found in high abundance in three out of four microhabitats, comprising ~10% of the total assemblages at the reference site, in-ref and microbial mat, but was nearly absent in the tubeworm zone. This morphotype has a subspherical agglutinated test, with a characteristic neck tapering towards the aperture.

Allogromiids encased in sediments, called mudballs (Fig. 25g), were found in high abundance in the reference zone, with abundance declining towards the microbial mat, where it was almost absent. These are identified as subspherical and largely featureless clumps of fine sediment, unconsolidated and prone to break when touched with picks or brushes.

Psammophaga sp. (Fig. 23j) was largely absent from the two reference sites, but abundant in both the tubeworm zone and the microbial mat, comprising 15% of the total assemblage in the latter sample. The species has a finely agglutinated and oval test, tapering towards the apertural end.

White saccamminid 1 (Fig. 23c-e) was common in all microhabitats except for the microbial mats, comprising ~1% of the total assemblage. This morphotype has an oval to droplet-shaped test of fine quartz grains and a prominent apertural neck. Although it has no assigned "working" morphospecies known from the literature, it is morphologically similar to the unidentified saccamminid 2 found in Majewski *et al*. (2005). It is distinguishable from the

white saccamminid 2 (Fig. 23h), occurring at the reference site and the in-ref, by the presence of a distinct apertural neck.

Unidentified saccamminid 1 (Fig. 27a-c) occurred only in the microbial mat, where it was highly abundant and comprised 23% of the total assemblage. This morphotype, undescribed in the literature, has an approximately dome-shaped test of fine agglutinated material and is found attached to larger quartz grains.

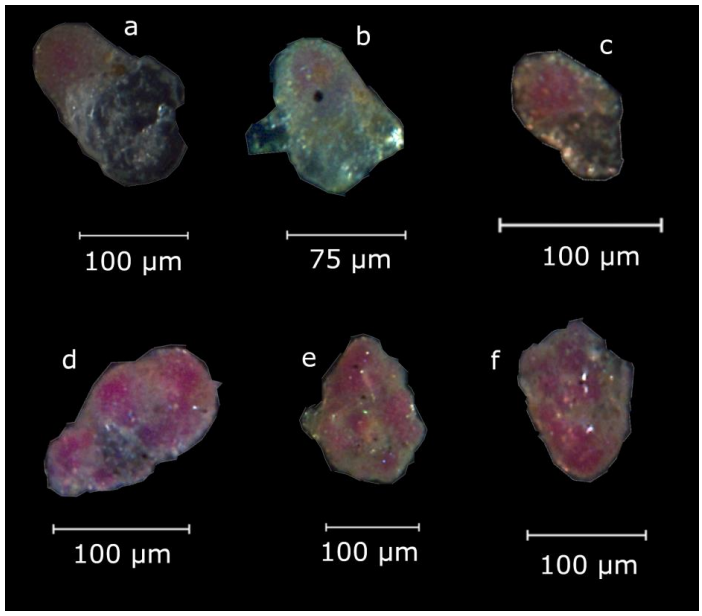

Figure 27: Unidentified saccamminids. a-c: Unidentified saccamminid 1 attached to grains. d: Cluster of Unidentified saccamminid 1. e-f: Unidentified saccamminid 2.

Saccamminid sp. 6e (Fig. 23i,n). occurred in moderate abundance in the in-ref, tubeworm zone and microbial mat. As seen in Sabbatini et al. (2007), this morphospecies has an agglutinated oval test, similar to *Psammophaga sp.*, but with less tapering towards the aperture, and a rougher surface texture. The large cytoplasm and slightly opaque test is comparable to the psammosphaerids.

Psammosphaerid sp. 1 (Fig. 24a), the second most abundant psammosphaerid, occurred in moderate abundance across all samples. It is morphologically similar to Psammosphaerid sp. 4, but with a thicker agglutinated test.

Unidentified saccamminid 2 (Fig. 27e-f), like unidentified saccamminid 1, occurred only in the microbial mat, where it was found in great abundance, comprising ~17% of the total assemblage. It has a rough surface texture, with a patchy agglutinated test covering the inner organic layer. The shape is roughly oval, tapering towards a presumed aperture.

Saccamminid sp. 17, as seen in Sabbatini *et al*. (2007), occurred in limited abundance in the in-ref, tubeworm zone and microbial mat. This morphotype has a thin test of relatively coarse material arranged in a plate-like manner giving it a distinct surface texture. In some specimens, two apertures were observed.

The multilocular agglutinated species were mostly represented by members of the genus *Rheophax* (Fig 26), with *R. guttifer* (Brady, 1881) being most abundant, though still very rare with eight total specimens identified, all within the reference site.

5.4 Diversity indices

Taxonomic richness varied amongst the sites, with the highest richness observed at the tubeworm zone with a total of 26 identified species, and the lowest at the mat with 14 (Fig. 28). The reference site had a slightly higher taxonomic richness than at the in-ref, with 22 and 18 identified taxa, respectively. The Shannon-Wiener index was fairly stable, for the first three sites with H'=2,63 at the reference site, 2,79 at the in-ref and 2,77 at the tubeworm zone. A significant drop is observed at the microbial mat, with H'=2,23 (Fig. 28). Fisher's α fluctuated among the sites, starting at α=6,9 at the reference site, decreasing to 4,9 at the in-ref, increasing to 8,4 at the tubeworm zone, before dropping down to 3,5 at the microbial mat Fig. 28). Interestingly, the evenness (J') is comparatively high for the in-ref at J'=0,96 while stable at all other sites at ~0,85 (Fig. 28). Simpsons index of diversity (1-D) shows a small rise from the reference site to the in-ref, at 1-D=0,90 and 0,93, respectively, before showing a declining trend towards the microbial mat, with 0,91 and 0,87 for the tubeworm zone and the microbial mat, respectively (Fig. 28).

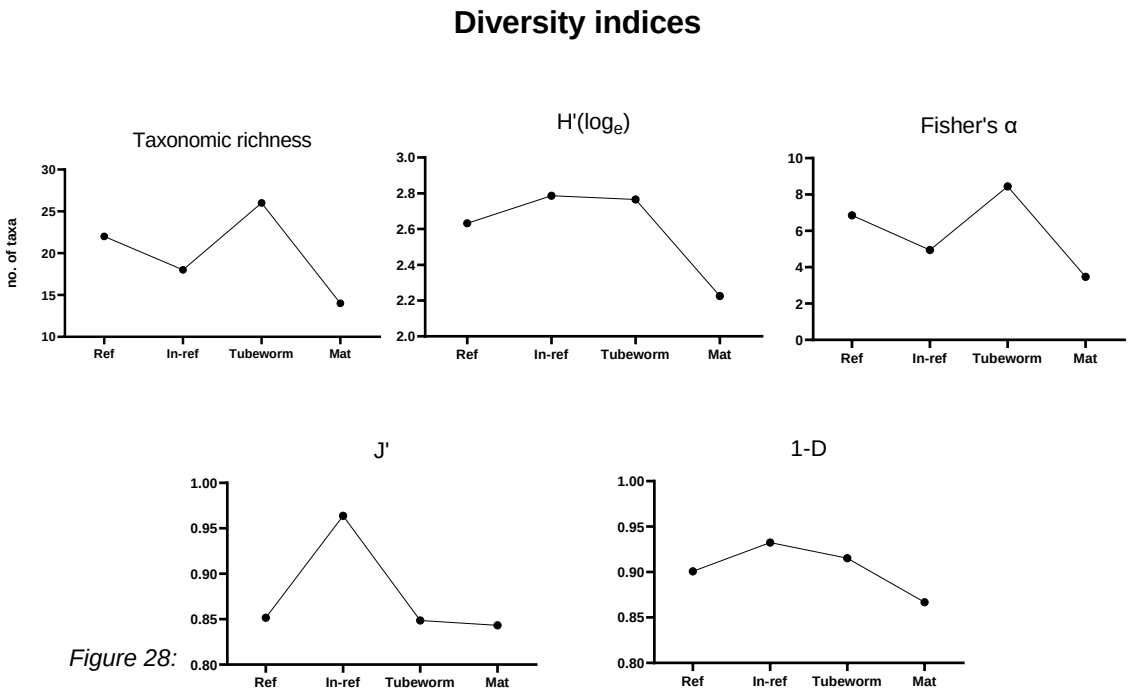

Figure 28:

Figure 28: Biodiversity indices calculated for the morphologcial dataset.

Overall, the biodiversity indices indicate a comparatively lower diversity in the microbial mat. The highest diversity is observed in the tubeworm zone, and in the in-ref the specimens are most evenly distributed amongst the present species.

6 Discussion

6.1 Molecular studies

The high number of extraneous sequences belonging to *Stainforthia* could indicate some cross-contamination in the laboratory, as many *Stainforthia* specimens were also processed as part of the project. This highlights the importance of sterile lab conditions while carrying out DNA sequencing in the lab.

6.1.1 Epistominella exigua

Although spanning great geographical distances, *E. exigua* displays very low diversity across different populations. The newly obtained sequences are identical to the sequences obtained from the Northern Atlantic, and the sequences obtained from an abyssal population (>4650 m water depth) only differ by a single substitution (T->C) (Fig. 29). This is in line with previous studies by Pawlowski *et al*. (2007) and LeCroq *et al*. (2009), who hypothesized the four Weddell Sea specimens to represent a subpopulation undergoing speciation. Comparingly, the shallow-water species *E. vitrea* shows a higher degree of genetic diversity, across much smaller geographical distances (from Argentina to Antarctica) with a total of 36 single nucleotide polymorphisms (SNPs) identified through pairwise comparisons of the four sequences belonging to *E. vitrea*.

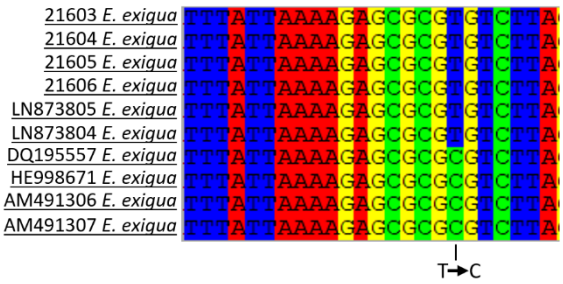

Figure 29: Parts of sequences belonging to the E. exigua used in the phylogeny, showing the single substitution (T->C) differentiating the abyssal Weddell Sea population from other E. exigua.

While the uniformity of deep-sea environments might result in global genetic homogeneity (LeCroq *et al*. 2009), cold-seep environments with their stronger environmental gradients and unique associated communities, might provide the ecological niche for genetic differentiation. However, all sequences of *E. exigua* obtained for this study are from the reference site, and more sequences would need to be obtained to look into this.

Overall, the phylogenetic analysis clearly distinguishes the sequences down to species-level to a satisfying degree (Fig.18).

6.1.2 Bolivina pseudopunctata

Some genetic differentiation is observed within the 3 newly obtained sequences, likely due to natural genetic variation. Some divergence is observed from the other *B. pseudopunctata* included in the analysis, indicating some genetic heterogeneity across geographical distance or between environments. Unfortunately, sampling depth was not available for the other *B. pseudopunctata* from Gullmar Fjord, and no other confirmed *B. pseudopunctata* sequences were available from the BLAST database for further comparison. Foraminifera sp. N10 from off-shore Namibia likely represents a closely associated species or perhaps even *B. pseudopunctata*, although no further information was available on this sequence.

Overall, the phylogenetic analysis manages to distinguish the sequences down to species-level to a satisfying degree (Fig 19).

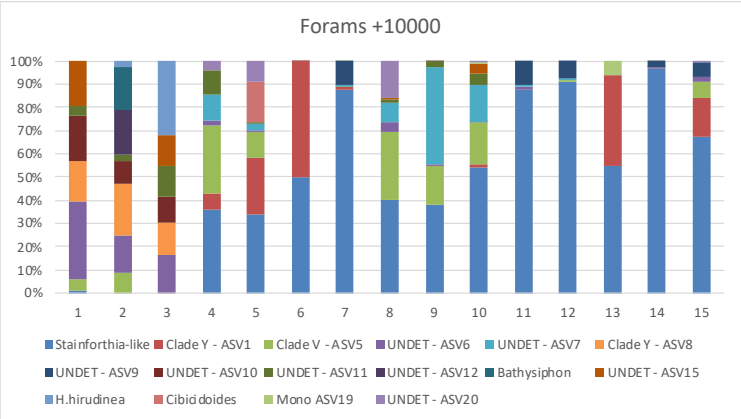

Figure 30: Taxonomic composition of most abundant foraminifera ASVs (>10000 reads) at various oil- and methane seep sites near Svalbard, including Svyatogor ridge (Stations 5-7). Note the abundance of Stainforthia-like sequences, as well as the many undetermined ASVs.
Source: Progress report by Pawlowski et al. commissioned by Giuliana Panieri for the AKMA project.

6.1.3 Stainforthia cf. fusiformis

The interest in the genus *Stainforthia* in relation to seep environments was spurred by a pilot study by Pawlowski *et al*. (Unpublished, progress report commissioned by Prof. Giuliana Panieri on behalf of the AKMA project), which reported an abundance of *Stainforthia*-like

sequences obtained from Illumina high-throughput sequencing of sediments from cold seeps at varying sites, including Svyatogor Ridge (Fig. 30).

The six newly obtained sequences show an overall genetic homogeneity across all sampling habitats, with only three incidents of SNP, likely due to natural genetic variation.

Evolutionary relationships are not immediately clear based on the phylogeny, with complex branching patterns and no clear distinction between the sequences assigned to *S. fusiformis* and *Stainforthia* sp. (Fig. 20). Even the placement of *F. complanata* outside the clade comprising all *Stainforthia* sequences is very poorly resolved at BV = 17. The newly obtained sequences show a high genetic similarity to sequences assigned to both *Stainforthia sp.* and *S. fusiformis* but based on available information on sampling localities and water depths of sequences used in the phylogeny, no trends become immediately clear. Unlike the two previous phylogenies in this study that successfully resolved species-level evolutionary relationships, this particular phylogeny only managed to resolve a single species relationship to a satisfying degree, with the grouping of the two Northern Atlantic *S. fusiformis* sequences within group 1 (Fig. 20).

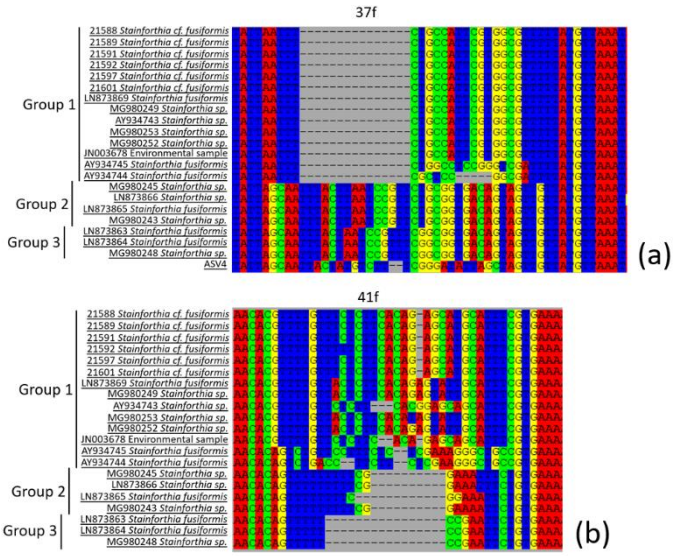

Figure 31: parts of the 37f (a) and 41f (b) foraminifera-specific variable regions, showing some molecular diversity in the Stainforthia sequences used in the phylogeny (Fig. 7). a: Groups 2, 3 and the ASV differs from group 1 with varied insertions, prolonging the region. b: Group 1 differs from group 2 and 3 by varied insertions, prolonging the region.

A closer look at the sequences reveals some similarities within the 3 groups. Figure 31 shows the two foraminifera-specific hypervariable regions 37f and 41f. Group 2 and 3 appear to differ from group 1 by a 15 bp long insertion in the 37f region (Fig. 31a). Conversely, group 1 differs from group 2 and 3 with a highly variable insertion in the 41/f region (Fig. 31b). Members of the same shallow-water population (Beagle Strait, 44 m water depth, accession nos. MG980248-MG980253) can be observed in both group 1 and 3, possibly indicating

cryptic speciation or at least high molecular diversity even at a small geographical scale. A study by Majda *et al*. (2018) divided *Stainforthia* sequences (including the previously mentioned Beagle Strait population) obtained from across the Drake Passage into 4 molecular operational taxonomic units (MOTUS), with up to 7% genetic dissimilarities within the populations. This is in contrast to the *Epistominella* genus, displaying a largely global genetic homogeneity with clear species delineation (Fig. 18). Overall, the available sequences do not seem to provide a clear delineation of the molecular boundaries of the species *S. fusiformis*, as evident from the phylogeny (Fig. 20) and sequence differences (Fig. 31).

The ASV unexpectedly groups closest to the outgroup taxa, at the base of the tree (Fig. 20). This is likely an artifact caused by the sequence being rather short at 120 bp and only covering the 37f hypervariable region, and not containing enough variation to properly compare and distinguish it from other sequences.

Comparisons of the 37f region with other sequences (Fig. 31a) reveal that the ASV differs from the other newly obtained *Stainforthia* sequences with an insertion more akin to what is observed in the *Stainforthia* from group 2 and 3. This is indicative of several different genotypes of *Stainforthia* being present. An explanation for this variation could however also be intragenomic polymorphism. Weber & Pawlowski (2014) studied intragenomic polymorphism in SSU rDNA of Monothalamea and Globothalamea, including *S. fusiformis*. Here, a high level of intragenomic variability was observed, with a sequence divergence as high as 2,72 % found in *S. fusiformis*, based on a total of 68 clones of four specimens. For *S. fusiformis*, and Globothalamea in general, a high degree of this variability was observed in the 37f region (See Fig. 2 in Weber & Pawlowski, 2014).

Some efforts have been made to distinguish *S. fusiformis* from other morphologically similar *Stainforthia sp*. Gooday & Alve (2001) compared specimens of *S. fusiformis* from their typical coastal setting (55-203 m water depth, Norwegian waters) to a morphologically similar form, sampled from abyssal depths (4850 m water depth, Porcupine Abyssal Plain).

Though appearing highly similar, biometrics and morphological comparisons revealed subtle differences: *Size*. Specimens of *S. fusiformis* are larger than the abyssal form (80-380 μm for *S. fusiformis*, compared to 40-150 μm for the abyssal *Stainforthia sp.*). *Chamber morphology*. Chambers were generally found to be more elongated in *S. fusiformis*, with a greater degree of

overlap between chambers, in comparison to *Stainforthia sp*. *Pores*. Pores are generally larger and denser in tests of *S. fusiformis* compared to *Stainforthia sp. Apertural region*. The aperture in *S. fusiformis* is generally located further away from the end of the test in a prominent depression, bordered by a serrated toothplate. In *Stainforthia sp.* the depression is not as well developed, the aperture is located more towards the terminal end and the toothplate is not serrated and more linear. For a more in-depth description of these features and differences, refer to Gooday & Alve (2001)

When comparing the newly obtained specimens (Fig. 14, Plate 1) with the material from Gooday & Alve (2001), the SEM micrographed specimens seem to fit the description of *S. fusiformis* better, based especially on the test lengths, greater size, and higher density of pores and the well-developed aperturial depression. A missing feature is the serrated toothplate, although many of the SEM micrographed specimens have damaged apertures or have the aperture hidden away from view. Though *S. fusiformis* are more commonly found in coastal to outer shelf bathymetric ranges (Gooday & Alve, 2001), reports of *S. fusiformis* down to 2200 m water depth in the Northern Atlantic (Austin & Evans, 2000).

Based on available molecular data as well as morphological comparison, the *Stainforthia* specimens obtained in this study are (cautiously) identified as *Stainforthia cf. fusiformis*.

Why the single-cell DNA extraction of these particular specimens only seem to record the genotype missing the 37f insertion remains a question. One possibility could be that the genotype recorded in the metabarcoding studies represent the morphologically distinct and smaller *Stainforthia sp.*, while the barcoded specimens represent *Stainforthia cf. fusiformis.* The smaller *Stainforthia sp.* could be present in the smallest sieve fraction (<63 µm), that wasn't studied closely under microscope.

Stainforthia sp. could also be present in the form of propagules, small juvenile forms in a dormant stage, measuring just 10s of microns (Alve & Goldstein, 2003). *Stainforthia sp*., similar to *E. exigua,* are opportunists, often found in areas characterized by a seasonal input of phytodetritus, for example provided by a seasonal algal bloom. Seasonal dormancy has been reported in other Rotaliids (Ross & Hallock, 2016), and it is possible that *Stainforthia sp.* could be present in a resting stage, waiting for an input of phytodetritus. In the Arctic, a

seasonal bloom of phytoplankton is observed in early July (Søreide *et al*. 2010), occurring after the sampling occurred.

In any case, both genotypes are found across all microhabitats and thus neither seem to indicate a specific adaptation to seep environments.

6.1.4 Synthesis of molecular studies

The three species and their associated phylogenies represent different aspects of molecular foraminiferal studies. Genetically homogenous species like *E. epistominella* can easily be distinguished from other morphologically similar foraminifera, enabling identification. Cryptic speciation of isolated or ecologically restricted populations can be recognized for further studies. *Bolivina pseudopunctata* was upon first examination assigned to the genus *Brizalina*, however its close association with another *B. pseudopunctata* and the genus *Bolivina* in general ensured proper identification. For *S. fusiformis*, especially compared to *E. epistominella*, the molecular species delineation is not as apparent perhaps due to researchers' caution with assigning species to taxa with a high degree of genetic polymorphism. Here integrative taxonomy, the combination of morphological and molecular data **(**Dayrat, 2005), allowed for distinguishing of two morphologically similar species.

This form of barcoding study serves only to identify the species inhabiting this unique environment. All sequences will be made publicly available in a future publication, enabling other researchers in their studies of life in extreme environments. Contributions of barcodes of identified foraminifera is important, as molecular databases are key to eDNA studies, and for foraminifera this database is still lacking (Pawlowski & Holzmann, 2014). As of 2014, only ca. 1% of the foraminiferal species in the World Register of Marine Species had sequences assigned to them in publically available databases. (Pawlowski & Holzmann, 2014). Notice the large amount of undetermined ASVs in Fig. 30. The expansion of foraminiferal databases is an important task, especially given their usefulness in biomonitoring (Schönfeld, *et al*. 2012).

The interspecific variation reported in this study was low, indicating little to no genetic variation between microhabitats. However, to properly study genetic variation as an indicator of adaptation to different environments transcriptomics, the study of the combined RNA

transcripts in an organism (Lowe *et al*. 2017), is more suitable. This is however outside the scope of this thesis.

6.2 Morphological dataset

6.2.1 Biodiversity

Studies of diversity in monothalamous communities can be difficult to compare, in part due to differences in methodology (Goineau & Gooday, 2017). Sabbatini *et al*. (2007) studied living monothalamous assemblages in the inner Tempelfjord, Svalbard (water depth 26-104 m) and identified a total of 63 monothalamous species across nine sampling stations. Other studies of Arctic monothalamous assemblages such as Majewski *et al*. (2005) and Gooday *et al*. (2005) have mostly focused on the larger (125 µm+) fractions, however the latter study did identify 36 species in the 63-125 µm fraction. Though the sampling environments of the aforementioned studies differ from the current study, the 32 monothalamous types recognized in this study does seem a bit high in comparison, especially given the smaller sample size. It cannot be ruled out that the numbers presented here might be skewed due to lack of expertise with monothalamous foraminifera. One possible source of error could be the intraspecific morphological plasticity of some monothalamids (Goineau & Gooday, 2017) leading to members of the same species erroneously being recognized as different species. On the other hand, the contrast in taxonomic richness could also be due to greater differences in environmental parameters in the microhabitats studied in this thesis, as foraminifera are known for their high degree of specialization (Schönfeld et al 2012)

For an ecological study, the sample size of ~200 picked specimens per sample is in the low end. However, it should be sufficient for semi-quantitative comparisons of larger trends across the studied microhabitats and to highlight possible bioindicator species for future studies.

Removing the calcareous taxa drastically lowers the taxonomic resolution of the dataset (Fig. 21). The calcareous taxa are usually well-studied, and despite only accounting for 11% of the total dataset, made up for a substantial part of the species-assigned taxa in the dataset.

The low relative abundance of allogromiids is puzzling (Fig. 22). In the study by Sabbatini *et al.* (2007) allogromiids made up more than half of all monothalamids and one third of all live

foraminifera collected in Tempelfjord. In this study, allogromiids only made up ~12% of the samples, with a declining trend towards the microbial mat. One explanation could be that saccamminids are more common in this deep-water environment, or more tolerant to the harsh geochemical conditions in and around methane seeps. Perhaps, like the multilocular agglutinants, they are also mainly oligotrophs. It is also possible that the allogromiids don't preserve as well in ethanol in the long term. Examination of the samples didn't begin until roughly four months after collection and ended roughly 11 months after collection due to limited access to the microscope. In case the delicate allogromiids were degraded in this time, a considerable component of the foraminiferal assemblages could be missing due to preservation bias.

Some of the trends observed in this study are in line with previous studies. Dessandier *et al*. (2019) found that both abundance and diversity of foraminifera were lower in methane-charged sediments, and that agglutinated species were few or absent. For monothalamous foraminifera, the assemblage in the microbial mat showed the lowest diversity, and the abundance of multilocular agglutinated species gradually decreased from reference zone to microbial mats (Fig. 21). This decrease in abundance supports the hypothesis from ***et*** Dessandier *al*. (2019) that the oligotrophic multilocular agglutinants are limited by the eutrophic conditions of the seep environments at Vestnesa Ridge, something also observed at other methane seeps (Heinz *et al*. 2005; Panieri & Sen Gupta, 2008).

While the aforementioned hypothesis is seemingly true for multilocular agglutinants and maybe allogromiids as well, it does not explain the overwhelming abundance of soft-shelled agglutinants (Saccamminids and psammosphaerids) in the microbial mat, with the contribution of saccamminids increasing from reference zone to microbial mat (Fig. 21). Psaemmosphaerid sp. 4 and Saccamminid sp. 6 show considerable abundance across all microhabitats, indicating an ability to thrive across various trophic conditions. *Psammophaga sp.* shows a high abundance only in the tubeworm zone and microbial mats, while being rare to absent at the reference site and in the in-situ reference sampling site. This could indicate a tolerance for the eutrophic conditions found at methane seeps, and perhaps even a symbiotic relationship with methanotrophic bacteria, akin to what is suggested for *M. barleeanus* by Bernhard & Panieri (2018). In order to examine this, further analysis beyond the scope of this thesis would be needed, such as transmission electron miscroscopy.

The two undescribed saccamminids combined comprise 40% of the assemblage in the microbial mats and are completely absent from all other samples. They could potentially represent bioindicator species, highly specialized to the seep environment, such as the aforementioned symbioses with methanotroph bacteria. This claim would of course require more studies.

Though it is difficult to properly characterize the geochemical conditions of the sampling environment without proper analysis, some inferences can be made. The grey to black color of the microbial mats, as seen in Fig. 5e**,** indicate an unstable environment with transport of methane partially through advection in intense fluxes, as reported by Dessandier *et al*. (2019). The two undescribed saccamminids as well as *Psammosphaga sp.* seem to thrive in this hostile environment.

Based on the findings of the biodiversity data obtained from the morphological dataset, there seem to be potential in pursuing barcoding of saccamminids and psammosphaerids in hopes to improve the quality of future metabarcoding studies of the seep environments. To this measure, *Psammophaga sp.*, and in particular the two unidentified saccamminids stand out as prospective candidate species.

6.2.2 Monothalamids as a biomonitoring tool

The FOBIMO initiative (Schönfeld *et al*. 2012) does not recommend the use of soft-shelled foraminifera in foraminiferal biomonitoring studies, mostly due to the lack of consistent morphological identification, the arduous efforts to sort them and the limited knowledge on their distribution and ecology. While the author of this thesis can attest to several of the aforementioned statements, it is evident that monothalamids comprise a large portion of foraminiferal assemblages, and much information on biodiversity is lost by not considering this group. In the case of Goineau & Gooday (2017) it was estimated that up to 93% of the foraminiferal diversity would have been lost if the soft-shelled species had not been considered. Knowledge of soft-shelled foraminifera is ever expanding, including molecular phylogenetic analysis (Pawlowski *et al*. 2008) and more recent metabarcoding studies (Lejzerowicz *et al*. 2021). Sabbatini *et al*. (2013) found that 80% of the stained assemblage at a seep-influenced site in the Adriatic Sea consisted of soft-shelled foraminifera with Psammosphaerid sp. 1 representing ~50% of the assemblage, highlighting it's potential as a

bioindicator species of seep environments. Though Psammosphaerid sp. 1 doesn't show the same abundance in this study, several other species show a similar potential. Soft-shelled foraminifera are not preserved in the fossil record but could be useful in future ancient eDNA studies. Furthermore, the hostile conditions imposed by high pCO2 from methane oxidation has been found to limit or inhibit calcification of foraminiferal tests (Herguera *et al.* 2014) and favor agglutinated or organic-walled species.

6.3 Synthesis of methodologies

The datasets obtained and presented in this thesis are unique, as to my knowledge they represent the first characterization of a soft-shelled community sampled directly from a microbial mat exhibiting episodic seepage, as well as the first barcode sequences obtained from the seep-associated tubeworm zone. The aim of this thesis was to advance knowledge on methane-related foraminifera. It is my hope that the newly obtained knowledge presented here can prove useful in the further pursuit of a greater understanding of life in extreme environments.

The different methods employed in this thesis highlight very different aspects of foraminiferology and biodiversity studies in general. With the molecular approach, the concept of species is usually highly delineated, and when species is assigned, it is with great confidence. This can however also lead to reluctance in assigning species based on morphology alone.

In the case of morphology-based studies, informal groupings and morphotypes have little phylogenetic evidence, but is useful in studies of lesser studied groups, such as the ones presented in this thesis. However, it is time consuming and requires a high degree of expertise. It also does not account for cryptic speciation and in some cases morphological plasticity, which might lead to under- or overestimation in biodiversity studies.

The two methodologies complimented each other well in this study. The morphological approach, besides from providing valuable data in and of itself, also managed to highlight three particular candidate species for metabarcoding studies, as well spur an interest in the saccamminid group as a whole.

7 Conclusion

In summary, this thesis has explored foraminiferal biodiversity at Vestnesa Ridge from both a molecular and morphological perspective.

13 new sequences, obtained from the reference site, in-ref and tubeworm zone have been described and put into a phylogenetic perspective. *Epistominella exigua* displayed large genetic homogeneity and indicated no adaptation in response to environment. However this genetic homogeneity also makes it easy see when possible speciation arise. *Bolivina pseudopunctata* did not display much genetic variation, however, as only one other sequence assigned to *B. pseudopunctata* was publicly available, the addition of three more sequences is surely welcome. The new sequences belonging to *Stainforthia cf. fusiformis* also did not display much variance across microhabitats, but differed from the *Stainforthia* ASV obtained from metabarcoding studies, indicating the presence of another, perhaps smaller, *Stainforthia sp.*, a fact that would have been overlooked in morphological studies. All 13 sequences will help to expand the ever-growing database of foraminiferal sequences.

The morphological studies assessed the biodiversity of a group of foraminifera previously unstudied in Vestnesa Ridge. Some shifts were observed in foraminiferal assemblage and biodiversity indices across the microhabitats. Diversity fell with proximity to the microbial mat, in line with previous studies. Also in line with previous studies was the decrease in contribution of multilocular agglutinants to the faunal assemblage with proximity to the mat. This trend was also observed for the organic-walled allogromiids, perhaps indicating a similar ecological strategy. Psammosphaerids and saccamminids were abundant across all microhabitats, with the foraminiferal community at the microbial mat being largely made up of two undescribed saccamminids not present in other samples, indicating a high degree of specialization to the hostile environment, and a potential for future barcoding studies.

In future studies, the work in this thesis could be followed up in the multiple ways, including:

- More barcoding of seep foraminifera, as none of the foraminifera sampled from the microbial mats managed to sequence.
- More studies into the monothalamous assemblages of Vestnesa Ridge, as the sample size was rather low.

- Molecular studies of some of the lesser described monothalamous taxa to establish phylogenetic relationships and species delineation and expand the database of foraminifera adapted to extreme environments as a whole.
- Transcriptomic studies of seep-related foraminifera to uncover possible environmental adaptations.

8 References

Alve, E. & Goldstein, S.T. (2003) Propagule transport as a key method of dispersal in benthic foraminifera (Protista). *Limnology and Oceanography, vol. 48-6, pp. 2163-2170*. Association for the Sciences of Limnology and Oceanography.

Argentino, C., Savini, A. & Panieri, G. (2022) Integrating fine-scale habitat mapping and pore water analysis in cold seep research: A case study from the SW Barents Sea. In *World Atlas of Submarine Gas Hydrates in Continental Margins* (eds. Mienert, J., Berndt, C., Tréhu, A., Camerlenghi, A. & Liu, C.-S.), *pp, 505-515*. Springer Nature Switzerland.

Austin, W.E.N. & Evans, J.R. (2000) North East Atlantic benthic foraminifera: modern distribution patterns and palaeoecological significance. *Journal of the Geological Society, London, vol. 157, pp. 679-691*. Geological Society of London.

Brady, H.B. (1881) Notes on some of the Reticularian Rhizopoda of the "Challenger" Expedition. Part 3. *Quarterly Journal of Microscopial Science*.

Brady, H.B. (1884) Report on the foraminifera dredged by the H.M.S Challenger during the years 1873-1876. *Report on the scientific results of the voyage of H.M.S Challenger during the years 1873-76*.

Bernard, B.B., Brooks. J.M. & Sackett, W.M. (1978) Light hydrocarbons in recent Texas continental shelf and slope sediments. *Journal of Geophysical Research, vol. 83, pp. 4053-4061*. American Geophysical Union.

Bernhard, J.M. & Panieri, G. (2018) Keystone Arctic paleoceanographic proxy association with putative methanotrophic bacteria. *Scientific Reports, vol. 8.* Nature.

Bünz, S., Polyanov, S., Vadakkepuliyambatta, S., Consolaro, C. & Mienert, J. (2012) Active gas venting through hydrate-bearing sediments on the Vestnesa Rdige, offshore W-Svalbard. *Marine Geology, vols. 332-334, pp. 189-197*. Elsevier.

Cavanaugh, S.E. & Bathrick, A.S. (2018) Direct PCR amplification of forensic touch and other challenging DNA samples: A review. *Forensic Science International: Genetics, vol. 32, pp. 40-49*. Elsevier.

Cohen, J., Screen, J.A., Furtado, J.C., Barlow, M., Whittleston, D., Coumou, D., Francis, J., Dethloff, K., Enthekhabi, D., Overland, J. & Jones, J. (2014) Recent Arctic amplification and extreme mid-latitude weather. *Nature Geoscience, vol. 7, pp. 627-637.* Nature.

Cushman, J.A. (1922) Results of the Hudson Bay Expedition. The Foraminifera. *Contributions to Canadian Biology, vol. 9, pp. 133-147*.

Cushman, J.A. (1922) Foraminifera of the Atlantic Ocean. Part 3 – Textulariidae. *United States National Museum Bulletin, vol. 104, pp. 1-149.*

Cushman, J.A. (1926) Some Pliocene Bolivinas from California. *Contributions from the Cushman laboratory for foraminiferal research, vol. 2-2, pp. 40-47*.

Dayrat, B. (2005) Towards integrative taxonomy. *Biological Journal of the Linnean Society, vol. 85-3, pp. 407-417*. The Linnean Society.

Dessandier, P.-A., Borelli, C., Kalinitchenko, D. & Panieri, G. (2019) Benthic foraminifera in Arctic methane hydrate bearing sediments. *Frontiers in Marine Science, vol. 6.* Frontiers.

Egger, J.G. (1893) Foraminiferen aus Meeresgrundproben, gelothet von 1874 bis 1876 von S. M. Sch. ”Gazelle”. *Abhandlungen der Matematisch-Physikalischen Classe der Königlich Bayerischen Akademie der Wissenschaften*.

Farrell, E.M. & Alexandre, G. (2012) Bovine serum albumin further enhances the effects of organic solvants on increased yield of polymerase chain reaction of GC-rich templates. *BMC Research notes 5*. Springer Nature.

Francis, J.A., Vavrus, S.J. & Cohen, J. (2017) Amplified Arctic warming and mid-latitude weather: new perspectives on emerging connections. *Wiley Interdisciplinary Reviews: Climate Change, vol. 8.* Wiley Periodicals.

Frontalini, F., Cordier, T., Balassim E., Armynot du Chatelet, E., Cermakova, K., Apothéloz-Perret-Gentil, L., Martins, M.V.A., Bucci, C., Scantamburlo, E., Treglia, M., Bonamin, V. & Pawlowski, J. (2020) Benthic foraminiferal barcoding and morphology-based assessment around three offshore gas platforms: Congruence and complementarity. *Environment International, vol. 144.* Elsevier.

Gascuel, O. (1997) BIONJ: An improved version of the NJ algorithm based on a simple model of sequence data. *Molecular Biology and Evolution, vol. 14-7, pp. 685-695.*Oxford University Press.

Goineau, A. & Gooday, A.J. (2017) Novel benthic foraminifera are abundant and diverse in an area of the abyssal equatorial Pacific licensed for polymetallic nodule exploration. *Scientific reports, vol. 7*. Nature.

Gooday, A.J. (1986) Meiofaunal foraminiferans from the Bathyal Porcupine Seabight (Northeast Atlantic): Size structure, standing stock, taxonomic composition, species diversity and vertical distribution in the sediment. *Oceanographic Research Papers, vol. 33-10, pp. 1345-1355, 1357-1373*. Elsevier.

Gooday, A.J. & Alve, E. (2001) Morphological and ecological parallels between sublittoral and abyssal foraminiferal species in the NE Atlantic: A comparison of *Stainforthia fusiformis* and *Stainforthia sp. Progress in Oceanography, vol. 50, pp. 261-283*. Elsevier.

Gooday, A.J. (2002) Biological responses to seasonally varying fluxes of organic matter to the ocean floor: A review. *Journal of Oceanography, vol. 58, pp. 305-332*. Springer.

Gooday, A.J., Bowser, S.S., Cedhagen, T., Cornelius, N., Hald, M., Korsun, S. & Pawlowski, J. (2005) Monothalamous foraminiferans and gromiids (Protista) from western Svalbard: A preliminary survey. *Marine Biology Research, vol. 1, pp. 290-312*. Taylor & Francis.

Gouy, M., Guindon, S. & Gascuel, O. (2010) SeaView version 4: A multiplatform graphical user interface for sequence alignment and phylogenetic tree building. *Molecular biology and evolution, vol. 27-2, pp. 221-224*. Oxford Academic Press.

Guindon, S., Dufayard, J.F., Lefort, V., Anisimova, M., Hordijk, W. & Gascuel, O. (2010) New algorithms and methods to estimate maximum-likelihood phylogenies: Assessing the performance of PhyML 3.0. *Systematic Biology, vol. 59-3, pp. 307-321*. Oxford University Press.

Haacke, R.R., Westbrook, G.K. & Hyndman, R.D. (2007) Gas hydrate, fluid flow and free gas: Formation of the bottom-simulating reflector. *Earth and Planetary Science Letters*. Vol. 261-3-4. Elsevier.

Hayward, P.J. & Ryland, J.S. (1990) The marine fauna of the British Isles and North-West Europe. Volume 1: Introduction and Protozoans to Arthropods. Oxford University Press.

Heinz, P., Sommer, S., Pfannkuche, O. & Hemleben, C. (2005) Living benthic foraminifera in sediments influenced by gas hydrates at the Cascadia convergent margin, NE Pacific. *Marine Ecology Progress series, vol. 304, pp. 77-89*. Inter-Research Science Publisher.

Herguera, J.C., Paull, C.K., Perez, E., Ussler III, W. & Peltzer, E. (2014) Limits to the sensitivity of living benthic foraminifera to pore water carbon isotope anomalies in the methane vent environments. *Paleoceanography and Paleoclimatology, vol. 29-3, pp. 273-289*. American Geophysical Union.

Höglund, H. (1947) Foraminifera in the Gullmar Fjord and the Skagerak. *Zoologiska bidrag från Uppsala, vol. 26, pp. 1-328*.

Jackson, R.B., Solomon, E.I., Canadell, J.G., Cargnello, M. & Field, C.B. (2019) Methane removal and atmospheric restoration. *Nature Sustainability, vol. 2, pp. 436-438.* Nature.

Joung, DJ., Ruppel, C., Southon, J., Weber, T.S. & Kessler, J.D. (2022) Negligible atmospheric release of methane from decomposing hydrates in mid-latitude oceans. *Nature Geoscience, vol. 15, pp. 885-891*. Nature.

Knittel, K. & Boetius, A. (2009) Anerobic oxidation of methane: Progress with an unknown process. *Annual Review of Microbiology, vol. 63, pp. 311-334*. Annual Reviews.

LeCroq, B., Gooday, A.J. & Pawlowski, J. Global genetic homogeneity in the deep-see foraminiferan *Epistominella exigua* (Rotaliida: Pseudoparrellidae)*. *Zootaxa vol. 2096, pp. 23-32*. Magnolia Press.

Lefort, V., Longueville, J.-E. & Gascuel, O. (2017) SMS: Smart Model Selection in PhyML. *Molecular Biology and Evolution, vol. 1-34, pp. 2422-2424*. Oxford University Press.

Lejzerowicz, F., Gooday, A.J., Angeles, I.B., Cordier, T., Morard, R., Apothéloz-Perret-Gentil, L., Lins, L., Menot, L., Brandt, A., Levin, L.A., Arbizu, P.M., Smith, C.R. & Pawlowski, J. (2021) Eukaryotic biodiversity and spatial patterns, in the Clarion-Clipperton Zone and other abyssal regions: Insights from sediment DNA and metabarcoding. *Frontiers in Marine Science, vol. 8*. Frontiers.

Majda, A., Majewski, W., Mamos, T., Grabowski, M., Godoi, M.A. & Pawlowski, J. (2018) Variable dispersal histories across the Drake Passage: The case of coastal benthic foraminifera. *Marine Micropaleontology, vol. 140, pp. 81-94*. Elsevier.

Majewski, W., Pawlowsk, J. & Zajaczkowski, M. (2005) Monothalamous foraminifera from West Spitsbergen fjords, Svalbard: An overview. *Polish Polar Research, vol. 26-4, pp. 269-285*. Polska Akademika Nauk.

Mau, S., Römer, M., Torres, M.E., Bussmann, I., Pape, T., Damm, E., Geprägs, P., Wintersteller, P., Hsu, C.-W., Loher, M. & Bohrmann, G. (2017) Widespread methane seepage along the continental margin off Svalbard – from Bjørnøya to Kongsfjorden. *Scientific Reports, vol. 7.* Nature.

Montagu, G. (1803) Testacea Britannica or natural history of British shells, marine, land and fresh-water, including the most minute: Systematically arranged and embellished with figures.

Mullis, K.B. & Faloona, F. (1987) Specific synthesis of DNA *in vitro* via a polymerase catalyzed chain reaction. *Methods in Enzymology, vol. 155, pp. 335-350*. Academic Press.

Ogden, R.C. & Adams, D.A. (1987) Electrophoresis in Agarose and Acrylamide gels. *Methods in Enzymology, vol. 152, pp. 61-87*. Academic Press.

Orbigny, A.D.d'. (1826) Tableau méthodique de la classe des Cépahlopodes. *Annales des Sciences Naturelles, vol. 7*.

Panieri, G. (2006) Foraminiferal response to an active methane seep environment: A case study from the Adriatic Sea. *Marine Micropaleontology, vol. 61-1-3. pp. 116-130*. Elsevier.

Panieri, G. & Sen Gupta, B.K. (2008) Benthic foraminifera of the Blake Ridge hydrate mound, Western North Atlantic Ocean. *Marine Micropaleontology, vol. 66-2, pp. 91-102*. Elsevier.

Panieri, G., Graves, C.A. & James, R.H. (2016) Paleo-methane emissions recorded in foraminifera near the landward limit of the gas hydrate stability zone offshore western Svalbard. *Geochemistry, Geophysics, Geosystems, vol. 17, pp. 521-537*. American Geophysical Union.

Panieri, G., Bünz, S., Fornari, D.J., Escartin, J., Serov, P., Janson, P., Tores, M.E., Johnson, J.E., Hong, WL, Sauer, S., Garcia, R. & Gracias, N. (2017) An integrated view of the methane system in the pockmarks at Vestnesa Ridge, 79N. *Marine Geology, vol. 390*. Elsevier.

Panieri, G., Bünz, S., Savini, A., Jensen, A., Løfquist, B., Olsen, B.R., Willis, C., Argentino, C., Bertin, C., Oddone, D., Kalenitchenko, D., Rosnes, E., Cusset, F., Maric, F., Franchi, F., Pawlowski, J., Zimmermann, J., Todd, J.E., Meyer, J.P., Waghorn, K.A., Losleben, L.K., Poto, M.P., Eilertsen, M.H., Stiller-Reeve, M.A., Clerici, M., Dessandier, P.-A, Moncelon, R., Ramalho, S., Mohadjer, S., Vågenes, S., Aune, V., Os, V., Poddevin, V., Holm, V.D. (2022) CAGE22-2 Scientific Cruiste Report: AKMA2/OceanSenses. *CAGE – Centre for Arctic Gas Hydrate, Environment and Climate report series, vol. 10*.

Parker, F.L. (1953) North Atlantic Foraminifera. Reports of the Swedish deep sea expedition 1947-1948.

Parr, W.J. (1950) Foraminifera. *B.A.N.Z Antarctic Research Expedition 1929-1931. Report*.

Pawlowski, J. (2000) Introduction to the Molecular Systematics of Foraminifera. *Micropaleontology, vol. 46, supplement 1: Advances in the Biology of foraminifera, pp. 1-12*. The Micropaleontology Project, Inc.

Pawlowski, J. & Holzmann, M. (2002) Molecular phylogeny of foraminifera – a review. *European Journal of Protistology, vol. 38-1, pp. 1-10*. Elsevier.

Pawlowski, J., Fahrni, J., LeCroq, B., Longet, D., Cornelius, N., Excoffier,, L., Cedhagen, T. & Gooday, A.J. (2007) Bipolar geneflow in deep-sea benthic foraminifera. *Molecular ecology, vol. 16-19, pp. 4089-4096*. Wiley.

Pawlowski, J., Majewski, M., Longet, D., Guiard, J., Cedhagen, T., Gooday, A.J., Korsun, S., Habura, A.A. & Bowser, S.S. (2008) Genetic differentiation between Arctic and Antarctic monothalamous foraminiferans. *Polar Biology, vol. 31, pp. 1205-1216*. Springer.

Pawlowski, J. & LeCroq, B. (2010) Short rDNA barcodes for species identification in foraminifera. *The journal of Eukaryotic Microbiology, vol. 57-2, pp. 197-205*. International Society of Protistologists

Pawlowski, J., Esling, P., Lejzerowicz, F., Cedhagen, T. & Wilding, T.A. (2014) Environmental monitoring through protist next.generation sequencing metabarcoding: assessing the impact of fish farming on benthic foraminifera communities. *Molecular Ecology Resources, vol. 14-6, pp. 1129-1140*. Wiley.

Pawlowski, J. & Holzmann, M. (2014) A plea for DNA barcoding of foraminifera. *Journal of Foraminiferal Research, vol. 44-1, pp. 62-67*. Cushman Foundation for Foraminiferal Research.

Pawlowski, J., Cermakova, K. & Apothéloz-Perret-Gentil, L. (2022) Environmental DNA metabarcoding of sediment samples from Arctic extreme ecosystems. *Progress report commissioned by Prof. Giuliana Panieri*. ID-Gene ecodiagnostics, unpublished.

Plaza-Faverola, A., Bünz, S., Johnson, J.E., Chand, S., Knies, J., Mienert, J. & Franek, P. (2015) Role of tectonic stress in seepage evolution along the gas hydrate-charged Vesnesa Ridge, Fram Strait. *Geophysical Research Letters, vol. 42-3*. American Geophysical Union.

Plaza-Faverola, A. (2022) CAGE21-5 Cruise Report: Test of offshore instrumentation for in-situ sediment pressure measurements, west-Svalbard continental margin. *CAGE – Centre for Arctic Gas Hydrate, Environment and Climate report series, vol. 9*

Ross, B.J. & Hallock, P. (2016) Dormancy in the foraminifera: A review. *Journal of Foraminiferal Research, vol. 46-4, pp. 358-368*. Cushman Foundation of Foraminiferal Research.

Rouse, G.W. (2001) A cladistic analysis of Sibonoglidae Caullery, 1914 (Polychaeta, Annelida): Formerly the phyla Pogonophora and Vestimentifera. *Zoological Journal of the Linnean Society, vol. 132-1*. The Linnean Society of London.

Sabbatini, A., Morigi, C., Negri, A. & Gooday, A.J. (2007) Distribution and biodiversity of stained monothalamous foraminifera from Tempelfjord, Svalbard. *Journal of Foraminiferal Research, vol. 37-2, pp. 93-106*. Cushman Foundation for Foraminiferal Research.

Sabbatini, A., Nardelli, M.P., Morigi, C. & Negri, A. (2013) Contribution of soft-shelled Monothalamous taxa to foraminiferal assemblages in the Adriatic Sea. *Acta Protozoologica, vol. 52, pp. 181-192*. Jagiellonian University.

Sanger, F., Nicklen, S. & Coulson, A.R. (1977) DNA sequencing with chain-terminating inhibitors. *Proceedings of the National Academy of Sciences, vol. 74-12, pp. 5463-5467*. National Academy of Sciences.

Schochetmann, G., Ou, C.-Y. & Jones, W.K. (1987) Polymerase Chain Reaction. *The Journal of Infectious Diseases, vol. 158-6, pp. 1154-1157*. Oxford University Press.

Schönfeld, J., Alve, E., Geslin, E., Jorissen, F., Korsun, S., Spezzaferri, S. (2012) The FOBIMO (FOraminiferal BIo-MOnitoring initiative – Towards a standardized protocol for soft-bottom benthic foraminiferal monitoring studies. *Marine Micropaleontology, vol. 94-95, pp. 1-13*. Elsevier.

Serreze, M.C. & Barry, R.G. (2011) Processes and impacts of Arctic amplification: A research synthesis. *Global and Planetary change, vol. 77, pp. 85-96*. Elsevier.

Søreide, J.E., Leu, E., Berge, J., Graeve, M. & Falk-Petersen, S. (2016) Timing of blooms, algal food quality and *Calanus glacialis* reproduction and growth in a changing Arctic. *Global Change Biology, vol. 16-11, pp. 3154-3163*. Wiley.

Totomoch-Serra, A., Marquez, M.F. & Cervantes-Barragán, D.E. (2017) Sanger sequencing as a first-line approach of Andersen-Tawil Syndrome. *F1000Research, vol. 6*. F1000research.

Uchio, T. (1962) Influence of the river Shinano on foraminifera and sediment grain size distribution. *Publications of the Seto Marine Biological Laboratory, vol. 10, pp. 363-392*.

Vanneste, M., Guidard, S., Mienert, J. (2005) Bottom-simulating reflections and geothermal gradients across the western Svalbard margin. *Terra Nova, vol. 17-6, pp. 510-516*. Wiley.

Vella, P. (1957) Studies in New Zealand foraminifera. Part 1 – foraminifera from Cook Strait. Part 2 – Upper Miocene to recent species of the Genus *Notorotalia*. *New Zealand Geological Survey Paleontological Bulleting, vol. 28, pp. 1-64*.

Vogt, P.R., Crane, K., Sundvor, E., Max, M.D. & Pfirman, S.L. (1994) Methane-generated(?) pockmarks on young, thickly sedimented oceanic crust in the Arctic: Vestnesa Ridge, Fram Strait. *Geology, vol. 22-3, pp. 255-258*. The Geological Society of America.

Weber, A.A.-T. & Pawlowski, J. (2014) Wide occurrence of SSU rDNA intragenomic polymorphism in foraminifera and its implifications for molecular species identification. *Protist, vol. 165-5, pp. 645-661*. Elsevier.

Whiticar, M.J. (1999) Carbon and hydrogen isotope systematics of bacterial formation and oxidation of methane. *Chemical geology, vol. 161-1-3, pp. 291-314*. Elsevier.

Williamson, W.C. (1858) On the recent Foraminifera of Great Britain. *The Ray Society, London, pp. 1-107*.

Winton, M. (2006) Amplified Arctic climate change: What does surface albedo feedback have to do with it? *Geophysical Research Letters, vol. 33-3*. American Geophysical Union.

Yang, S. & Rothman, R.E. (2004) PCR-based diagnostics for infectious diseases: Uses, limitations, and future applications in acute-care settings. *The Lancet – Infectious Diseases, vol. 4-6, pp. 337-348*. Elsevier.

Yao, H., Nieman, H. & Panieri, G. (2020) Multi-proxy approach to unravel methane emission history of an Arctic cold seep. *Quaternary Science Reviews, vol. 244*. Elsevier.

Electronic sources:

https://blast.ncbi.nlm.nih.gov/Blast.cgi - Basic Local Alignment Search Tool, National Center for Biotechnology Information

9 Appendix

Appendix 1 - protocol for guanidine extraction (All protocols provided by Maria Holzmann

Guanidin extraction

Material:

Extraction tubes and pestles , 0.5ml tubes, isopropanol, 70% ETOH, TE-buffer

Maximum speed: 14000rpm

1) Transfer a foraminifera into a tube containing 50ul guanidin using a minimum volume of sea water (3-5ul)
2) Grind specimen with a pestle if necessary
3) Heat for 15 min at 60°C .
4) To remove debris, centrifuge at 8000rpm for 1 min and transfer 40 ul of the supernatant into a new 0.5ml tube
5) Add 1ul of Glycoblue to each tube
6) Add the same volume of isopropanol as guanidine (40ul) to each tube and mix by vortexing
7) Let precipitate overnight at -20°C
8) Centrifuge 20min at maximum speed
9) Remove supernatant, take care to not touch or remove the pellet
10) Wash pellet with 100ul 70% ETOH
11) Centrifuge 1min at maximum speed
12) Remove supernatant, take care to not touch or remove the pellet
13) Dry pellet for 25-30 min at 30°C until all ethanol has evaporated
14) Dissolve pellet in 20ul TE buffer, keep in the refrigerator at least for 1hour or overnight, vortex from time to time.
15) Store extractions at -20°C.

Guanidin solution for a totale volume of 212 ml

- 100ml H2O, double distilled
- 100g Guanidinium isothiocyanate
- 10.6ml Tris 1M pH 7.6
- 4.25ml EDTA 0.5M

Warm 10’ at 60-70°C, dissolve with stirring then add:

- 4.24g of Sarkosyl (N-Lauroylsarcosine sodium salt)

- 2.1ml β-mercaptoethanol

Adjust to 212 ml with distilled H2O and preserve at 4°C

Appendix 2 – Protocol for DNeasy extraction

Before starting: Turn on heat block, adjust the temperature to 65°C

Take an aliquot of the elution buffer AE and preheat to 65°C

Centrifuge the tube with RNase shortly and put it on a rack

Prepare and number all tubes (lilac and white spin columns each with collection tubes and one extra collection tube per sample, 1.5ml tubes; you need two 1.5ml tubes per sample)

Transfer 675ul buffer AW1 in 1.5ml tubes and close them

1) Add 400ul Buffer AP1 to an extraction tube 1.5ml
2) Add one or several cells
3) Crush the cells with a pestle
4) Add 4ul RNasa A solution to each tube and vortex
5) Incubate the mixture for 10min at 65°C. Mix 2 or 3 times during incubation by inverting the tube
6) Add 130ul Buffer P3 to the lysate, mix and incubate 5min on ice
7) Centrifuge at maximum speed for 5min
8) Pipet the lysate into the QIAshredder Minispin column (lilac) placed in a 2ml collection tube without disturbing the cell-debris pellet and centrifuge for 2min at maximum speed
9) Transfer the flow-through into the tube that contains the buffer AW1 and mix by pipetting.
10) Pipet 650ul of the mixture into the DNEasy Minispin column (white) placed in a 2ml collection tube. Centrifuge 1min at 8000rpm
11) Discard flow-through. Repeat step 10 with remaining sample. Discard flow-through and collection tube.
12) Place the DNEasy Mini spin column into a new 2ml collection tube, add 500ul Buffer AW2 and centrifuge 1min at 8000rpm. Discard flow-through
13) Add 500ul Buffer AW2 to the DNEasy Mini spin column and centrifuge for 2min at maximum speed.
14) Transfer the DNEasy Mini spin column to a 1.5ml tube and pipet 50ul of preheated Buffer AE directly onto the DNEasy membrane. Incubate for 5min at RT and then centrifuge for 1min at 8000rpm to elute.

Appendix 3 – PCR and amplification protocol.

PCR Mix for one tube:

Before preparing the mix, vortex buffer, dNTP's, primers, BSA and the DNA extracts.
NEVER vortex the Taq Polymerase!

Work on ice!

- H2O bidistilled: 19.5ul
- Buffer (10x): 2.5ul
- dNTP's (10mM): 0.5ul
- Primer1(10pm): 0.5ul
- Primer2(10pm): 0.5ul
- BSA (20mg/ml): 0.5ul
- Taq polymerase: 0.1ul
- DNA sample: 1ul

For more than one PCR, prepare a master mix, vortex and distribute 24ul into each tube; add then 1ul of extracted DNA to each tube, close and vortex each tube, do the PCR.

AMPLIFICATION:

Hotlid: 105°C

1: 95°C - 60 sec

2: 94°C-30 sec

3: 50°C-30 sec

4: 72°C-90sec

Go to 2-34x

5: 72°C-3min

REAMPLIFCATION:

Hotlid: 105°C

1: 95°C-60-sec

2: 94°C-30 sec

3: 52°C-30 sec

4: 72°C-90 sec

Go to 2-24x

5: 72°C-3min

For the reamplifiction prepare the same master mix as for the first amplification, distribute it into the PCR tubes and add 1ul of the product from the first amplification to each tube.

Appendix 4 – Counting table/morphological dataset

Taxa	Ref	In-ref	Tubeworm zone	Mat
Psaemmospherid sp. 1	9	12	5	7
Psaemmespherid sp. 2	7	13	5	2
Psaemmospherid sp. 3	10	8	3	8
Psaemmospherid sp. 4	12	15	26	18
Psaemmespherid sp. 5	0	11	2	1
Psaemmospherid sp. 7	0	0	4	0
Psaemmospherid sp. 8	0	0	1	0
Psaemmospherid A	2	0	0	0
Saccamminid sp. 6	20	23	3	19
Saccamminid sp. 6e	0	13	7	14
Saccamminid sp. 7	1	0	20	0
Saccamminid sp. 12	11	0	12	0
Saccamminid sp. 14	0	0	7	0
Saccamminid sp. 17	0	12	10	9
White saccamminid 1	11	9	26	2
White saccamminid 2	7	16	0	0
Elongate silver saccamminid	2	0	2	0
Elongate saccamminid	0	0	1	0
Brown saccamminid w/o tube	8	0	0	5
Psammosphaga sp.	6	0	17	29
Conqueria-like sp	0	7	0	0
Psammosphaga 2	0	3	1	0
Phainogullmia sp	0	0	1	0
Unidentified saccamminid 1	0	0	0	44
Unidentified saccamminid 2	0	0	0	32

Mudball allogromiid	37	15	9	2
Allogromiid sp 5	0	0	1	0
Allogromiid sp 7	0	9	4	0
Allogromiid sp G	1	0	0	0
Goodayia sp.	1	0	1	0
Vanhoeffenella sp	2	0	0	0
Vellaria sp	0	5	0	0
Rheophax sp.	0	6	3	0
Rheophax guttifer	8	0	0	0
Rheophax subfusiformis	2	0	2	0
Rheophax nodulosa	1	6	0	0
Bathysiphon sp	4	0	2	0
Hippocrepinella hirudinea	1	0	0	0
S. fusiformis	6	5	8	0
B. pseudopunctata	2	0	1	0
B marginata	0	0	1	0
B skagerakkensis	0	0	1	0
G turgida	8	2	2	0
B frigida	3	0	1	0
Lagena sp.	0	0	7	8
Lagena striata	2	0	0	0
Lagena sp. 2	0	3	0	0
M. barleeanus	3	0	1	0
Spirophthalmidium acutimargo	10	0	0	0
E exigua	1	0	0	0
C wuellerstorfi	2	0	0	0
Bucella tenerrima	1	0	0	0
N labradorica	3	0	0	0
C reniforme	0	5	0	0
Dentalina sp.	0	2	0	0

Appendix 5 - Overview of sequences used in phylogenetic analysis

*****Own specimens marked with isolate no.

Species	Accession/isolate* no.	Sampling locality	Sampling depth (m)
Bolivina argentea	JQ013745	Santa Barbara Basin, USA	430
Bolivina cacozela	LN886734	New Zealand	N/A
Bolivina pseudopunctata	ON818347	Gullmar Fjord, Sweden	N/A
Bolivina pseudopunctata	**21539**	Vestnesa Ridge, Arctic Ocean	1390
Bolivina pseudopunctata	**21540**	Vestnesa Ridge, Arctic Ocean	1390
Bolivina pseudopunctata	**21547**	Vestnesa Ridge, Arctic Ocean	1390
Bolivina sp. FF65	LN886737	New Zealand	N/A
Bolivina sp. FF126	LN886738	New Zealand	N/A
Bolivina sp. FF127	LN886739	New Zealand	N/A
Bolivina subaerenensis	AY465838	Eastern Pacific	779
Bolivina subaerenensis	AY465839	Eastern Pacific	779
Bolivina subaerenensis	AY465840	Eastern Pacific	779
Environmental sample	JN003678	Sea of Japan	976
Epistominella exigua	**21603**	Vestnesa Ridge, Arctic Ocean	1380
Epistominella exigua	**21604**	Vestnesa Ridge, Arctic Ocean	1380
Epistominella exigua	**21605**	Vestnesa Ridge, Arctic Ocean	1380
Epistominella exigua	**21606**	Vestnesa Ridge, Arctic Ocean	1380
Epistominella exigua	AM491306	Weddell Sea, Antarctica	> 4650
Epistominella exigua	AM491307	Weddell Sea, Antarctica	> 4650
Epistominella exigua	DQ195557	Weddell Sea, Antarctica	> 4650
Epistominella exigua	FJ185800	Pacific Ocean	1990
Epistominella exigua	FJ185805	Pacific Ocean	1905
Epistominella exigua	FJ185806	Pacific Ocean	1905
Epistominella exigua	HE998671	Weddell Sea, Antarctica	>1200
Epistominella exigua	LN873804	Northern Atlantic	N/A
Epistominella exigua	LN873805	Northern Atlantic	N/A
Epistominella sp. 1	FJ185807	King George Island, Antarctica	107
Epistominella sp. 1	FJ185808	King George Island, Antarctica	108
Epistominella sp. 1	FJ185812	King George Island, Antarctica	100
Epistominella sp. 2	FJ185813	King George Island, Antarctica	100
Epistominella sp. 2	FJ185817	Ushuaia, Argentina	20
Epistominella sp. 3	FJ185820	Pacific Ocean	1110
Epistominella vitrea	AM491308	McMurdo Sound, Antarctica	200-1200
Epistominella vitrea	AM491311	Weddell Sea, Antarctica	0-200
Epistominella vitrea	AM491312	McMurdo Sound, Antarctica	200-1200
Epistominella vitrea	LN873812	Ushuaia, Argentina	N/A

Foraminiferan sp. N10	FM999849	Atlantic Ocean	N/A
Fursenkoina complanata	ON818446	Gullmar Fjord, Sweden	N/A
Liebusella goesi	FR754402	Oslo Fjord, Norway	157
Stainforthia fusiformis	**21588**	Vestnesa Ridge, Arctic Ocean	1397
Stainforthia fusiformis	**21589**	Vestnesa Ridge, Arctic Ocean	1397
Stainforthia fusiformis	**21591**	Vestnesa Ridge, Arctic Ocean	1380
Stainforthia fusiformis	**21592**	Vestnesa Ridge, Arctic Ocean	1380
Stainforthia fusiformis	**21597**	Vestnesa Ridge, Arctic Ocean	1400
Stainforthia fusiformis	**21601**	Vestnesa Ridge, Arctic Ocean	1380
Stainforthia fusiformis	AY934744	Skagerrak, Sweden	N/A
Stainforthia fusiformis	AY934745	Dunstaffnage, Scotland	N/A
Stainforthia fusiformis	HE998670	Skagerrak, Sweden	N/A
Stainforthia fusiformis	HG425204	Sweden	N/A
Stainforthia fusiformis	LN873863	Ushuaia, Argentina	N/A
Stainforthia fusiformis	LN873864	Ushuaia, Argentina	N/A
Stainforthia fusiformis	LN873765	Ushuaia, Argentina	N/A
Stainforthia fusiformis	LN873869	Tierra Del Fuego, Argentina	N/A
Stainforthia sp.	AY934743	Spitsbergen, Svalbard	N/A
Stainforthia sp.	MG980243	Admiralty Bay, Antarctica	119
Stainforthia sp.	MG980245	Admiralty Bay, Antarctica	119
Stainforthia sp.	MG980248	Beagle Strait, Chile	44
Stainforthia sp.	MG980249	Beagle Strait, Chile	44
Stainforthia sp.	MG980252	Beagle Strait, Chile	44
Stainforthia sp.	MG980253	Beagle Strait, Chile	44
Stainforthia sp.	LN873866	Ushuaia, Argentina	N/A
Trifarina earlandi	LN873502	McMurdo Sound, Antarctica	17
Trifarina earlandi	MG980241	Beagle Strait, Chile	16
Trochammina hadai	MZ707234	Australia	N/A
Trochammina inflata	MZ707245	Germany	N/A